Making Small Holes With Lasers

By

Jeffrey F. Herbstman

**A dissertation submitted in partial fulfillment
of the requirements for the degree of
Doctor of Philosophy
(Applied Physics)
in The University of Michigan
2010**

Doctoral Committee:

**Associate Professor Alan J. Hunt, Chair
Professor Roy Clarke
Professor Steven M. Yalisove
Adjunct Associate Professor John A. Nees**

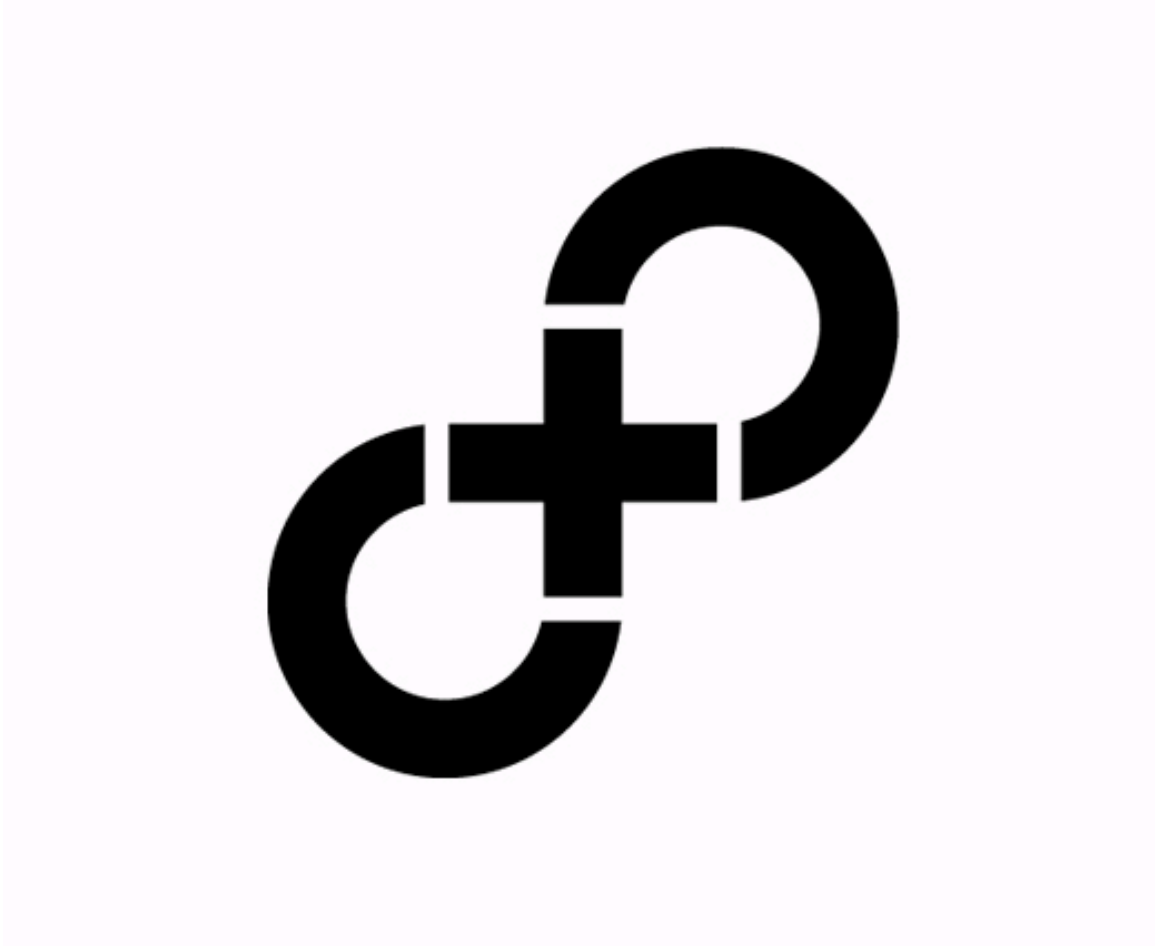

Acknowledgements

Science is not done in a vacuum. Well, some is. But even that science requires the effort and collaboration by a large number of people. I would like to thank the large number of people who have made the work I have presented here possible. First and foremost, my advisor and chair, Alan Hunt, has provided guidance, mentorship and support. He has tirelessly revised my writing, reviewed my results and sculpted my research so that it has formed a coherent body of work. Steven Yalisove has been an invaluable collaborator; insightful discussions with him regarding puzzling results are a major contribution to large portions of this work. John Nees has been the best resource possible for our laboratory regarding both ordinary and extraordinary occurrences with our laser science. His patient effort and knowledge has taught me much of what I know about working with lasers and optics. Roy Clarke has been involved in my Applied Physics career since I was first accepted into the program, as Program Chair, a member of my qualifying committee, and now a member of my thesis committee. I thank him for his support and effort on my behalf.

Some of my most rewarding experiences at the University of Michigan have been my interactions with members of the Hunt lab. Whether instructing a physicist on how to do biology, discussing papers at lab meeting, critically reviewing each others presentations or taking a short break together from our work, they have been some of the most patient, caring and helpful colleagues one might have asked for. Blake, David, Kevin, Jun, Ran and Seth, thank you. Finally, Damon Hoff deserves a separate, deep and heartfelt thanks. In sharing an office with Damon for the past few years, we have gotten to know each other well, sharing triumphs, failures and laughs. Not only are you a great friend, but you have also been a mentor and teacher. You have fixed the laser for me, and taught me to fix it for others. Our discussions on my work have been invaluable and our conversations on graduate school, science, and life have kept me sane.

There have been a number of collaborators on this research who have put in significant effort towards obtaining the enclosed results. First, without the preliminary work on this topic by Ajit Joglekar, none of this research would have been possible. Our collaborator examining the theoretical aspects of tightly focused femtosecond laser damage, Sergey Kudryashov, was the first author on the paper regarding the first discovery of the nanochannels and has provided vital discussion and guidance on this topic. Joel McDonald and Ryan Murphy contributed to the work preparing Silicon/Silicon Dioxide microfludic samples and working towards developing biological applications. Erik Yusko and Michael Mayer have been the major collaborators providing equipment, expertise and guidance for measuring the aforementioned samples. Many of the images in this thesis were taken at the Electron Microscopy Analysis Laboratory and the Microscopy Image Analysis Laboratory. John Mansfield, Haiping Sun, and Sasha Meshinchi gave me the guidance and training for instruments in these labs.

My path to this point has been the product of several physicists who require mentioning. Nathan Unterman taught my first physics course. His humor, enthusiasm, patience, and teaching style kindled my passion for physics. The idea that one could match equations to the falling of a object or amount of force required to move a car, and even predict future behavior was akin to giving me the power to unlock the world's secrets. I have been enthralled ever since. My first participation in physics research was with the supporting and mentorship of Richard Haglund and his research group. In our pursuit of the nature of light-matter interactions, I found the rush of novel science, observing phenomena never before experienced. As a graduate student here at the University of Michigan, I finally reached the point where I couldn't easily master concepts and calculations required of me. Without the patience, support and friendship of the other Applied Physics students in my class, I never would have made it through those first few years here. The faculty and staff of the Applied Physics program has always been there for me, in particular, Charles, Cynthia and Duncan Steel, have provided support and assistance when I needed it.

Finally, my family deserves my utmost gratitude. I've somehow developed a priority for a weekly phone call during which, typically, very little of consequence is discussed, but is more important than anything to make with my two grandmothers. I manage to call my parents and brothers slightly less often, but despite my periods of being incommunicative and withdrawn, it has given me much comfort knowing that you are there for me. I know that I can call or come home at any time and I will be welcomed. Thank you for being there for me.

Preface

The knowledge and results shown here are the product of a long process. One that began with the small experiment kits and chemistry sets of my youth. It continued with my science classes throughout elementary, middle and high school where I learned that I possessed an aptitude for science. An early disappointment in introductory chemistry confirmed that my real interest was in physics and the quantification and exploration of the world around me. Throughout my undergraduate years, I realized my passion for working in a laboratory and performing experiments. It seemed like a natural fit to continue my studies in graduate school. After a failed attempt to start these studies at the Technion in Israel, I was pleased to enter into the Applied Physics program at the University of Michigan.

I struggled through my first two years of courses, some requiring pages of derivations, novel strategies for approaching solutions and a great deal of learning from my Applied Physics colleagues. In between homework sets and exams, I started experiments in Prof. Hunt's lab, where I continued through my entire career at the University of Michigan. My explorations of the laser damage studied in his lab created the results shown in this dissertation. At times, I have doubted how much I was learning as I continued during my Ph.D. There were certainly times when grinding out long integrals late at night or when the laser was broken for months on end when I was frustrated to the point of tears. There were also times when I sat for hours measuring damage or taking electron micrographs, when I was sorely disappointed in the tedium that science had to offer. These difficulties serve to reinforce the idea that the successes, however small, should certainly be celebrated far more in science.

The day that I first imaged grommet formation, I knew I had taken a picture that would end up in this document. When I observed clear and interesting trends in nanochannel

formation, I knew I had found something meaningful. In retrospect, these actions, arriving at the end of exhausting days, deserved more than the shrug and the grin that they provided. I regret not greeting the publication of these data with more celebration. Too often, I found that by the time a paper was finally accepted, I was more tired of revising and refining its contents than realizing that it was the culmination of a large effort.

This text is a tangible product of those efforts; it contains much of the work I have performed during my Ph.D. career. However, I would like to believe that the knowledge and wisdom I have gained during this process would fill many more volumes. I have learned a great deal, from basic laser operation and repair to advanced electron microscopy. I have learned the rudiments of cellular biology, fluorescence microscopy and bicycle repair. I have met many great friends and colleagues, listened to dozens of seminars, and hopefully taken advantage of many of the wonderful opportunities this university has to offer.

As a fledgling scientist, I had hoped to make an important discovery that would revolutionize a field and, of course, get published on the cover of *Science* magazine. Although I have had to readjust my sights to a slightly lower aim, the work outlined in this volume describes my discovery of a number of phenomena that occur for tightly focused femtosecond laser damage and proposes physical mechanisms for their origin. I can only hope that my time spent on it was of use and that it serves a small purpose to illuminate a tiny region of the greater sphere of knowledge.

- J.F.H.

I thought that I'd lived long enough
that the light would come shining through,
but don't this look like the dark?
-Magnolia Electric Co.

Table of Contents

List of Figures:

Chapter 1

Introduction

> *Whatever is combustible flashes into flame at its touch, lead runs like water, it softens iron, cracks and melts glass, and when it falls upon water incontinently that explodes into steam.*

H.G. Wells' terrifying description of the Martian Heat-Ray in his 1898 novel, *War of the Worlds*, may be the first conception of the destructive power of laser technology. Indeed, once the laser was realized over 60 years later, it demonstrated its ability to damage metals, dielectrics and liquids as easily as Wells imagined. Although it was known for a time as a "solution looking for a problem," because of the uncanny ability of the laser to cause damage in a large range of materials, the study of its applications for material modification quickly became a promising field of research (Garwin and Lincoln 2003). This research has led to laser damage applications in fields including industrial manufacturing, surgery, exploring other planets and even fusion research.

The most vital precursor to the study of laser damage was the development and construction of the laser, first accomplished by Theodore Maiman in 1960 (Bertolotti 2005). Shortly following the invention of this device, reports of damage formed in transparent dielectrics were published (Grivet et al. 1964). As laser technology was refined and developed, the drive to achieve higher intensities became a goal of the field. Although stymied by optical damage effects from attempting to use conventional techniques to increase power, chirped pulse amplification (CPA) developed by Gerard Mourou and colleagues allowed the output power of lasers to increase by orders of magnitude (Strickland and Mourou 1985). This form of amplification allows high intensity, short duration pulses to be generated by a laser system. The availability of

lasers with pulses below a picosecond (10^{-12} seconds) and powers above one Terawatt (10^{12} Watts) led to the discovery of new laser damage physics in these regimes (Perry and Mourou 1994). Some of these new mechanisms for damage are outlined in the latter portion of Chapter 2.

Although CPA has been vital to techniques pushing the limits of laser output to 2 x 10^{22} W/cm^2, achieved at the University of Michigan's HERCULES facility (Yanovsky et al. 2008), the range of intensities required to start modifying materials is far more modest. These effects begin with temporary modifications of properties, including the index of refraction, molecular polarizibility, and transient changes in absorption, transmittivity and reflectivity (Wood 2003). As the intensity increases, material effects become permanent. These permanent changes define what is termed damage and will be the focus of this thesis.

Laser induced damage appears in a variety of forms and scales. On the atomic scale, crystalline phase changes can occur, dislocations and vacancies can be formed and migrate, and atoms can become ionized, among other effects. At larger, more macroscopic levels, laser damage can cause material to be cracked, melted, or removed.

While the ability of the laser to damage material may be a limiting factor for optical components, it also allows the laser to be used in a variety of applications. One such application that will be discussed at length in this dissertation is that of laser machining. The laser, especially when generating pulses below the picosecond time scale, is a unique tool for removing material and fabricating structures precisely, reproducibly and with superlative control. When this laser light is tightly focused, a number of novel, interesting features and mechanisms for damage arise. This dissertation endeavors to discuss and explain the physics that underlies tightly focused femtosecond laser damage and a some of its features and mechanisms.

This dissertation is organized in such a manner to guide the reader through the relevant history and physics of laser damage leading up to the work accomplished by the author.

It begins with a discussion of light propagation in transparent materials and nonlinear effects caused by laser propagation. It continues with sections on laser damage and the spectrum of mechanisms that lead to material modification, with a concentration on damage in transparent dielectrics. It then outlines the history of the effort to study the use of femtosecond laser damage to remove materials at the smallest scales possible, particularly for machining applications, including work accomplished at the University of Michigan demonstrating holes formed that are only tens of nanometers in diameter (Joglekar et al. 2003).

The sections that follow describe an exploration of the damage formed at small scales including descriptions of new and interesting behavior caused by femtosecond laser damage. A study of scaling behavior for damage formed using single pulses focused through different objective lenses shows a discontinuity in the expected relationship between damage width and pulse fluence. An investigation of this discontinuity illuminates the source as the generation of small, flat rings, termed "grommets", that can be ejected from regions surrounding the damage crater. A mechanism is proposed for the generation of these "grommets" (Herbstman et al. 2008).

Also described are measurements exploring the depth of damage produced with microscope objective lenses typically used for micromachining in glass. Conditions are discovered under which single pulse damage is formed that is much longer than the calculated and measured Rayleigh range of the objectives used. The nanochannels formed under these conditions are typically a few hundred nanometers wide and can be over five microns in depth. Possible physical mechanisms for this phenomenon are discussed (Kudryashov et al. 2007).

These nanochannels have a number of applications for which they are well suited. The first application presented is the use of these channels is for the generation of regular arrays of low volume wells. Another application is their use as out-of-plane vias or jumpers to complement existing and novel microfluidic fabrication techniques. Finally, potential future applications are suggested as directions for new and exciting research.

References

Bertolotti, Mario (2005), *The history of the laser* (Bristol ; Philadelphia: Institute of Physics Pub.) viii, 307 p.

Garwin, Laura and Lincoln, Tim (2003), *A century of nature : twenty-one discoveries that changed science and the world* (Chicago: University of Chicago Press) xviii, 360 p.

Grivet, Pierre, Bloembergen, N., and United States. Office of Naval Research. (1964), *Quantum electronics; proceedings of the third international congress. Électronique quantique; comptes-rendus de la 3e conférence internationale, Paris* (Paris, New York,: Dunod; Columbia University Press) 2 v. (xxix, 1923 p.).

Herbstman, J. F., Hunt, A. J., and Yalisove, S. M. (2008), 'Morphologies and nonlinear scaling of laser damage on glass surfaces by tightly focused femtosecond pulses', *Applied Physics Letters,* 93 (1).

Joglekar, A. P., et al. (2003), 'A study of the deterministic character of optical damage by femtosecond laser pulses and applications to nanomachining', *Applied Physics B-Lasers and Optics,* 77 (1), 25-30.

Kudryashov, S. I., et al. (2007), 'Nanochannels fabricated by high-intensity femtosecond laser pulses on dielectric surfaces', *Applied Physics Letters,* 91.

Perry, M. D. and Mourou, G. (1994), 'TERAWATT TO PETAWATT SUBPICOSECOND LASERS', *Science,* 264 (5161), 917-24.

Strickland, D. and Mourou, G. (1985), 'COMPRESSION OF AMPLIFIED CHIRPED OPTICAL PULSES', *Optics Communications,* 56 (3), 219-21.

Wood, Roger M. (2003), *Laser-induced damage of optical materials* (Series in optics and optoelectronics; Bristol: Institute of Physics) x, 241 p.

Yanovsky, V., et al. (2008), 'Ultra-high intensity-300-TW laser at 0.1 Hz repetition rate', *Optics Express,* 16 (3), 2109-14.

Chapter 2

Light Propagation in Transparent Dielectrics

This chapter discusses the propagation of light in materials. At low intensity regimes propagation can be considered a linear phenomenon. As the intensity of the light increases, the physics governing this propagation changes. Nonlinear effects become relevant and must be taken into account. Some of these nonlinear effects that will be discussed in later chapters are outlined below.

Light Propagation

Electromagnetic waves satisfy the following Maxwell's equations:

$$\begin{aligned} \nabla \cdot \boldsymbol{D} &= \rho & \nabla \cdot \boldsymbol{B} &= 0 \\ \nabla \times \boldsymbol{E} &= -\frac{\partial \boldsymbol{B}}{\partial t} & \nabla \times \boldsymbol{H} &= \frac{\partial \boldsymbol{D}}{\partial t} + \boldsymbol{J} \end{aligned} \tag{1}$$

In a nonmagnetic medium with no free charges or currents, the wave equation can be derived to the following form:

$$\nabla \times \nabla \times \boldsymbol{E} + \frac{1}{c^2}\frac{\partial^2 \boldsymbol{E}}{\partial t^2} = -\frac{1}{\epsilon_0 c^2}\frac{\partial^2 \boldsymbol{P}}{\partial t^2} \tag{2}$$

where $\boldsymbol{P}$ is the induced dipole moment vector or polarization, c is the speed of light and ε_0 is the permittivity of free space. For conventional optics the induced polarization can be described as "linear", as it depends linearly on the electric field, $\boldsymbol{E}$:

$$\boldsymbol{P}(t) = \epsilon_0 \chi^{(1)} \boldsymbol{E}(t) \tag{3}$$

where the constant of proportionality, $\chi^{(1)}$, is the linear susceptibility. This can be related to the commonly used refractive index, n_0, as follows:

$$n_0 = \sqrt{1 + \chi^{(1)}} \tag{4}$$

Nonlinear Optical Effects

As the intensity of light propagating through the medium increases, the linear approximation of polarization longer holds. Higher orders of the induced polarization are required and this property can be expressed in a Taylor series expansion:

$$\boldsymbol{P}(t) = \epsilon_0 \left[\chi^{(1)} \boldsymbol{E}(t) + \chi^{(2)} \boldsymbol{E}^2(t) + \chi^{(3)} \boldsymbol{E}^3(t) + \ldots \right] \tag{5}$$

$$\boldsymbol{P}(t) = \boldsymbol{P}^{(1)}(t) + \boldsymbol{P}^{(2)}(t) + \boldsymbol{P}^{(3)}(t) + \ldots \tag{6}$$

Where $\chi^{(2)}$, the second-order nonlinearity, is responsible for effects such as second-harmonic generation, sum and difference frequency generation and for parametric oscillation and amplification. The third order term, $\chi^{(3)}$, generates effects such as the Optical Kerr effect, third-harmonic generation, Raman and Brillouin scattering, self phase modulation and self-focusing (Boyd 2003). At the intensities reached by the lasers discussed in this thesis, further higher order terms can be ignored.

Second harmonic generation

One relevant nonlinear optical effect is that of second harmonic generation. This phenomenon occurs when a laser beam is incident on a crystal that has a non-zero second order susceptibility, $\chi^{(2)}$. The electric field can be represented as:

$$\boldsymbol{E}(t) = \boldsymbol{E}\, e^{-i\omega t} + c.c. \tag{7}$$

The nonlinear polarization that is created is of the following form:

$$\boldsymbol{P}^{(2)}(t) = 2\epsilon_0 \chi^{(2)} \boldsymbol{E}\boldsymbol{E}^* + \left(\epsilon_0 \chi^{(2)} \boldsymbol{E}^2 e^{-i2\omega t} + c.c.\right) \tag{8}$$

This equation shows a DC term and an additional term that contributes the frequency doubled component.

Figure 2.1 shows a cartoon of this process as two photons at the original laser frequency are converted into photons with twice the energy.

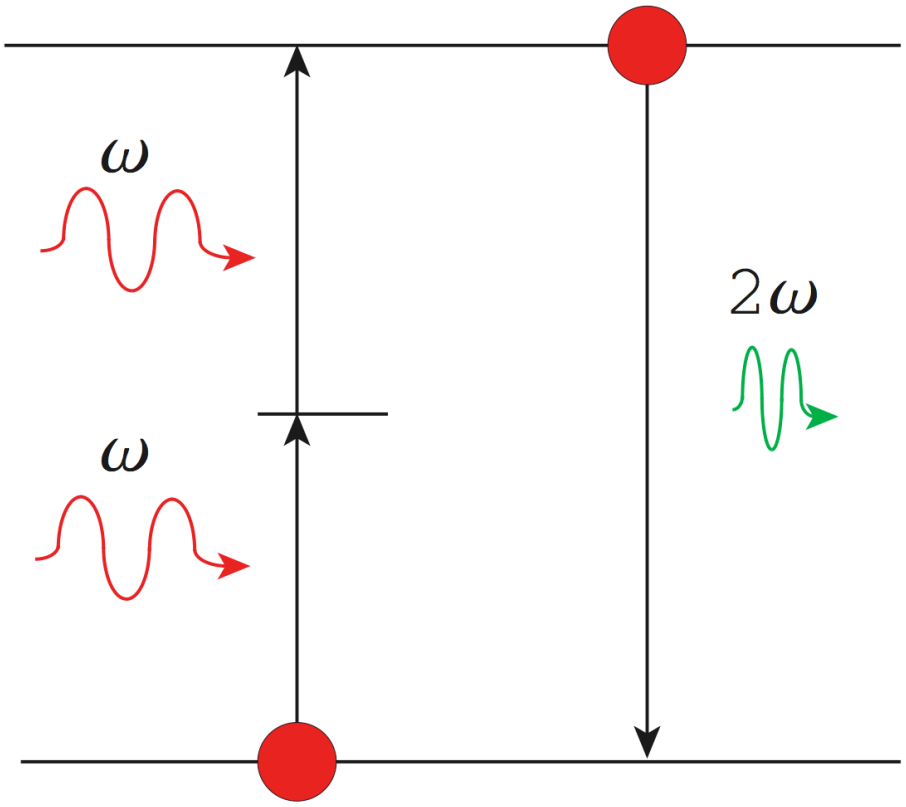

Figure 2.1. Second harmonic generation.

Self-focusing

Self-focusing, or Kerr focusing, is a process that occurs due to a positive nonlinear refractive index, n_2, also known as a Kerr index. This index is related to the third order susceptibility, $\chi^{(3)}$, which is present even in isotropic, amorphous materials such as glasses. This phenomenon is the result of a change in overall refractive index due to nonlinear changes from the intensity distribution of a laser beam, described by the following equation.

$$n = n_0 + n_2 I \tag{9}$$

The intensity towards the center of the beam causes an increase in this refractive index, acting as a lens to focus the light.

Plasma Defocusing

Ionization mechanisms discussed in the following chapter serve to generate a free electron plasma at the laser focus. The generation of this plasma causes a reduction of the index, effectively creating a negative lens to divert the beam outwards. This change can be described by the following equation:

$$n \simeq n_0 - \frac{\rho(r, t)}{2\rho_c} \tag{10}$$

where $\rho(r,t)$ is the density of free electrons and ρ_c, is the critical plasma density defined as $\rho_c = \varepsilon_0 m_e \omega_0^2 / e^2$ with m_e and e denoting the effective mass and charge of the electron and, ω_0, the laser frequency. The critical plasma density is the point above which the plasma becomes opaque to light, shielding the subsequent material (Schaffer 2001).

Filamentation

If the laser power is increased to a point where the strength of self-focusing is balanced by diffraction effects at the focus and plasma defocusing, the beam can exhibit long range, self-sustained behavior. The critical power for this behavior can be expressed as:

$$P_{cr} = \frac{\pi\,(0.61)^2\,\lambda_0^2}{8\,n_0\,n_2} \tag{11}$$

This phenomenon can confine the beam to narrow filaments that extend far beyond the Rayleigh length of the original focusing optics (Couairon and Mysyrowicz 2007).

References

Boyd, Robert W. (2003), *Nonlinear optics* (2nd edn.; San Diego, CA: Academic Press) xvii, 578 p.

Couairon, A. and Mysyrowicz, A. (2007), 'Femtosecond filamentation in transparent media', *Physics Reports-Review Section of Physics Letters,* 441 (2-4), 47-189.

Schaffer, C. B. (2001), 'Interaction of Femtosecond Laser Pulses with Transparent Materials', (Harvard University).

Chapter 3

Laser Damage Mechanisms

Laser damage in transparent dielectrics can take a variety of forms, including changes in reflectivity, transmittivity or absorption, crystalline phase changes, or physical modifications such as cracking, melting, shockwave propagation and material removal. This damage can occur both at the surface of the material and within the bulk. Depending on laser parameters such as pulse duration and shape, wavelength, and intensity, the mechanisms that cause this damage can be quite different. Broadly, damage mechanisms can be divided into two different categories, thermal absorption and dielectric breakdown.

Thermal Absorption

For continuous, long pulses (nanoseconds or longer), or successive short pulses at low intensity with respect to the threshold for damage that repeat on timescales short compared with the thermal dissipation time, the main mechanism for laser energy absorption and subsequent damage is via thermal mechanisms. A large number of material properties may influence absorption of laser light, including transmittivity, the presence of defects, microscale scratches or color centers, to name a few. Even in transparent materials, some amount of laser energy will be absorbed as heat. This deposition of thermal energy will cause the bulk temperature of the material to rise. This temperature rise may cause cracking due to thermal expansion as well as melting and vaporization.

Dielectric Breakdown

As J.J. O'Dwyer states in his monograph on dielectric breakdown, "All materials conduct electricity to a greater or lesser extent and all suffer some form of breakdown in a sufficiently strong electric field." Although these words were written in reference to DC breakdown, they are applicable to laser induced dielectric breakdown as well. The mechanisms for laser damage in transparent dielectrics were matched with mechanisms for electronic dielectric breakdown early on in the development of damage theory. Both forms are characterized by the inducement of a non-conductive material to allow current to pass in the presence of a strong field, causing the absorption of energy (O'Dwyer 1964).

Optical breakdown can be divided into two classes, avalanche ionization and multiphoton ionization/tunneling processes. Avalanche ionization describes the process in which carriers within the material, either intrinsically present due to thermodynamic distribution or defects, or extrinsically ionized carriers, gain energy and cause other carriers to become ionized. The free carriers present within the volume of laser irradiation are available to absorb photons. Once the energy gained by a carrier is larger than the band gap, it can interact with valence carriers in the bulk causing ionization. Each generation of ionization events doubles the number of free carriers within the material, leading to exponential growth. Once the free carrier density reaches the critical value of $\sim 10^{18}$ electrons/cm^3, dielectric breakdown occurs (Seitz 1949).

As the pulse duration of the laser is decreased below picoseconds, sufficient electrons in transparent dielectrics are not located within the interaction volume for successive generations of avalanche ionization to cause a critical density necessary for breakdown. In order for breakdown to occur, electrons for this process must be seeded via direct ionization processes. The two mechanisms for direct ionization are multiphoton absorption and Zener tunneling.

Multiphoton ionization (MPI) occurs when an electron is directly excited to the conduction band via the absorption of several photons until the energy that has been

gained is larger than the band gap and the electron is ionized. This process requires higher intensities than that of avalanche ionization, as the electrons must absorb several photons, enough to bridge the band gap, before relaxation or emission occurs. Electrons can also be directly ionized via Zener tunneling, a phenomenon where a strong electric field deforms the Coulomb potential well of the lattice to allow carriers to tunnel from potential wells to become free.

The degree to which multiphoton ionization and Zener tunneling occurs is indicated by the Keldysh coefficient. This unitless metric, originally calculated by L.V. Keldysh in 1964 for use in gases is given by the following equation:

$$\gamma = \frac{\omega}{e}\sqrt{\frac{m\,c\,n\,\epsilon_0\,E_g}{I}} \qquad (1)$$

where ω is the laser frequency, e and m are the effective charge and mass of the electron, c is the velocity of light, n is the index of refraction, ε_0 is the permittivity of free space, E_g is the band gap of the material and I is the laser intensity. For values of $\gamma >> 1$, multiphoton ionization is highly dominant for damage. A value of $\gamma << 1$ indicates that tunneling ionization is most prevalent (Keldysh 1965). The applicability of this coefficient in solids has called into question by Lenzner et al. who found that orders of magnitude lower ionization rates than the theory predicted by Keldysh (Lenzner et al. 1998), as well as by Joglekar et al. who found that damage threshold appears to be independent of polarization for a range of materials (Joglekar et al. 2004) however recent modifications of this model appear to reproduce experimental results accurately by taking into account crystalline solid band structure and the energy dependence of the effective mass for carriers (Gruzdev and Chen 2008).

The evidence for the role these different ionization mechanisms play in laser damage can be observed by examining the relationship between pulse duration, τ, and damage threshold. This relationship, at long pulse durations, can clearly be described by a $\tau^{-1/2}$ scaling law. This scaling can be explained as the effect of a diffusion limited thermal

conduction process. The dimension of the region where energy is deposited is on the order of $(D\tau)^{1/2}$ where D is the heat diffusion coefficient (Bloembergen 1997).

As the pulse duration decreases and reaches the order of 10^{-11} seconds, the threshold for damage deviates from this scaling law. This deviation is the result of the energy of the laser pulse being absorbed on a timescale faster than it can be deposited in the lattice. Thus, MPI/Tunneling becomes a mechanism for seeding the avalanche ionization that has limited by the duration of the pulse and therefore the build-up of free carriers. As the duration decreases further, ionization transitions to entirely multiphoton/tunneling processes (Lenzner et al. 1998; Stuart et al. 1996; Tien et al. 1999).

Additional evidence for a change in the mechanism for damage is found in the transition of damage from a probabilistic form, where damage appearance may occur for a range of intensities, to a deterministic form, showing generation of damage for all pulses above the damage threshold (Stuart et al. 1996). As the pulse duration approaches this transition, damage at longer pulse durations is stochastic; carriers may not be present within the focal region in sufficient amounts to fully ionize the material and cause damage. Ultrafast pulse damage, on the other hand, has a more deterministic character, with every pulse above threshold generating damage. Because each pulse generates free electrons, damage is mediated by the intrinsic properties of the material rather than stochastic number of seed electrons present in the focal volume due to defects, absorption centers, diffusion and thermally generated carriers that may or may not be present (Bloembergen 1974, Stuart et al. 1995).

The deterministic nature of this damage for femtosecond pulses at intensities above the threshold allows access to phenomena that push the boundaries of physics. Some of these phenomena allow novel techniques for manipulating matter and machining at small scales. These techniques will be discussed in the following chapter.

References

Bloembergen, .N (1974), 'Laser-Induced Electric Breakdown in Solids', *Ieee Journal of Quantum Electronics Qe10,* (3), 375-86.

Bloembergen, N. (1997), 'A brief history of light breakdown', *Journal of Nonlinear Optical Physics & Materials,* 6 (4), 377-85.

Gruzdev, V. E. and Chen, J. K. (2008), 'Laser-induced ionization and intrinsic breakdown of wide band-gap solids', *Applied Physics a-Materials Science & Processing,* 90 (2), 255-61.

Joglekar, A. P., et al. (2004), 'Optics at critical intensity: Applications to nanomorphing', *Proceedings of the National Academy of Sciences of the United States of America,* 101 (16), 5856-61.

Keldysh, L. V. (1965), 'IONIZATION IN FIELD OF A STRONG ELECTROMAGNETIC WAVE', *Soviet Physics Jetp-Ussr,* 20 (5), 1307-&.

Lenzner, M., et al. (1998), 'Femtosecond optical breakdown in dielectrics', *Physical Review Letters,* 80 (18), 4076-79.

O'Dwyer, John J. (1964), *The theory of dielectric breakdown of solids* (Monographs on the physics and chemistry of materials; Oxford,: Clarendon Press) viii, 142 p.

Seitz, F. (1949), 'On the Theory of Electron Multiplication in Crystals', *Physical Review,* 76 (9), 1376-93.

Stuart, B. C., et al. (1995), 'Laser-Induced Damage in Dielectrics with Nanosecond to Subpicosecond Pulses', *Physical Review Letters,* 74 (12), 2248-51.

Stuart, B. C., et al. (1996), 'Nanosecond-to-femtosecond laser-induced breakdown in dielectrics', *Physical Review B,* 53 (4), 1749-61.

Tien, A. C., et al. (1999), 'Short-pulse laser damage in transparent materials as a function of pulse duration', *Physical Review Letters,* 82 (19), 3883-86.

Chapter 4

Tightly Focused Femtosecond Laser Damage

The previous chapter outlines some of the mechanisms that make femtosecond laser damage distinct from other forms of laser damage. These mechanisms result in novel and unique forms of optical material modification that allow access to new applications for waveguides, micro- and nano-scale machining and material study. This chapter describes differences between the damage observed for ultrafast laser pulses and that of longer pulses. It then discusses particular unique effects achievable under tight focusing conditions and new techniques and applications of these effects.

Femtosecond Laser Damage Material Effects

When a laser impinges upon a surface of a material, energy is absorbed and the material is heated. For long pulses ($\tau > 1$ nanosecond) this energy is absorbed on the same time scale as the duration of the pulse and the region of the material that is heated through this process, the size of the Heat Affected Zone (HAZ), is mainly controlled by the material's ability to conduct heat away from the targeted region.

Within the HAZ, a wide range of material effects can be observed. These effects include ablation, melting, redeposition, recrystallization, cracking, and densification. For femtosecond laser damage these effects are not eliminated. However, for femtosecond pulse damage, energy is absorbed on a time scale shorter than that on which it can be transferred to the lattice. Thus, the HAZ is not mediated solely by thermal conductivity, but rather the size of the ionizing/absorbing region in the material from which heat is then radiated (See Figs. 1 and 2).

For femtosecond lasers, when the laser pulse hits the target, electrons can become ionized through the mechanisms described in the previous chapter. As this ionization occurs, the

material becomes highly absorbing until the point at which the critical density of free electrons is reached and a plasma is formed. This plasma is highly reflective and shields the material from the tail of the pulse, with the field only entering up to the effective skin depth, δ, where δ is:

$$\delta = \sqrt{\frac{2}{\mu\sigma\omega}} \qquad (1)$$

On the order of picoseconds, the highly energetic free electrons begin interacting with the atoms of the target. As the energy is transferred to the lattice, the material rapidly heats to a temperature well above the melting point. This superheated material is ejected in a plume of energetic plasma, the spectrum of which can provide important information on the material and ablation parameters, (Scaffidi et al. 2003). Outside the central region where material is fully removed, melt is also spallated and redeposited (Joglekar et al. 2003; Kudryashov et al. 2007). The Heat Affected Zone (HAZ) of this damage, in contrast with long pulse damage, can extend as little as a few nanometers from the damage region, as shown in Figure 4.2 (Stuart et al. 1996b). This minimization of the HAZ allows extremely precise machining and material modification (Pronko et al. 1995; Schaffer et al. 2001).

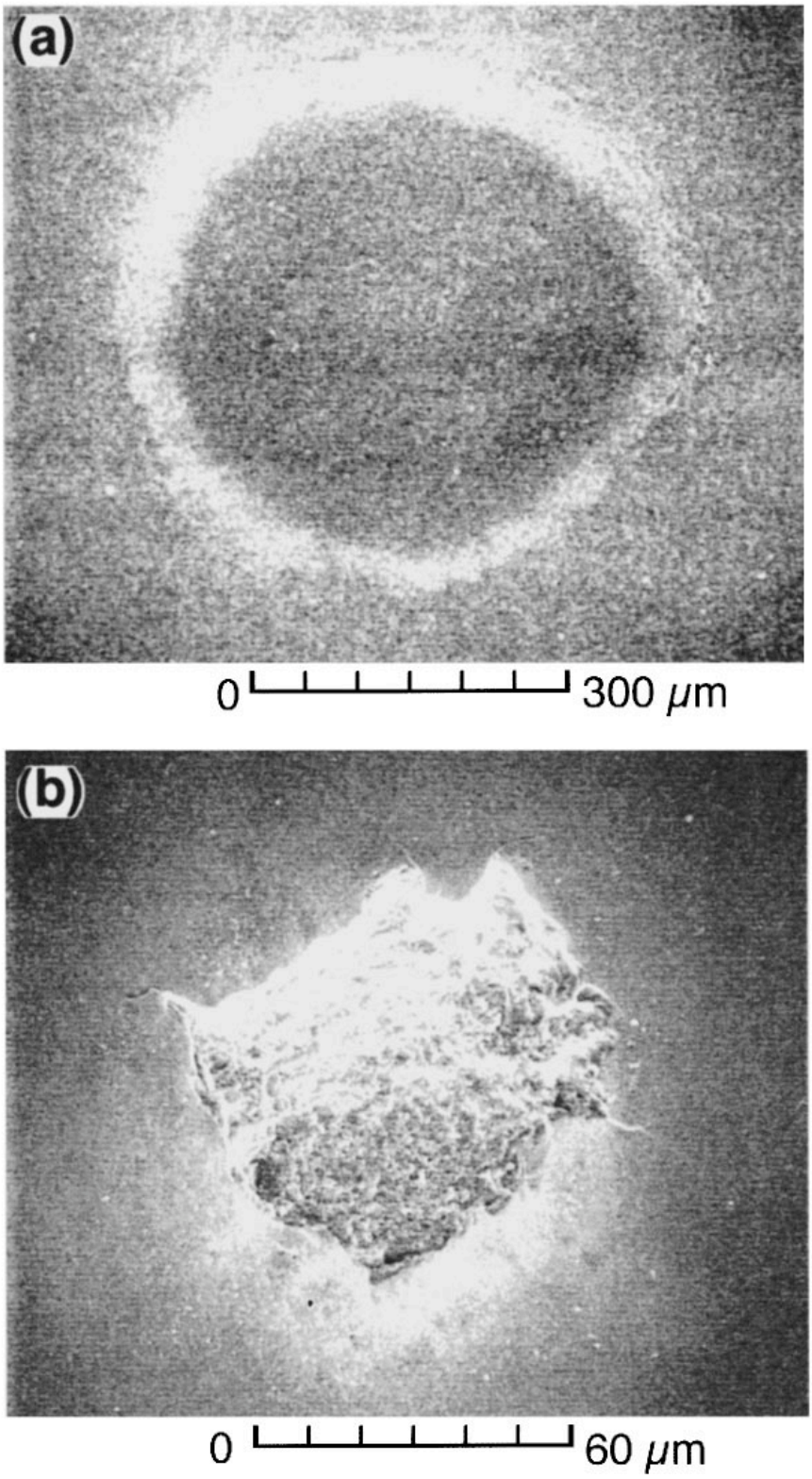

Figure 4.1. Laser damage spots on fused silica created by (a) a 900 picosecond pulse, (b) a 400 femtosecond pulse. From (Stuart et al. 1996b)

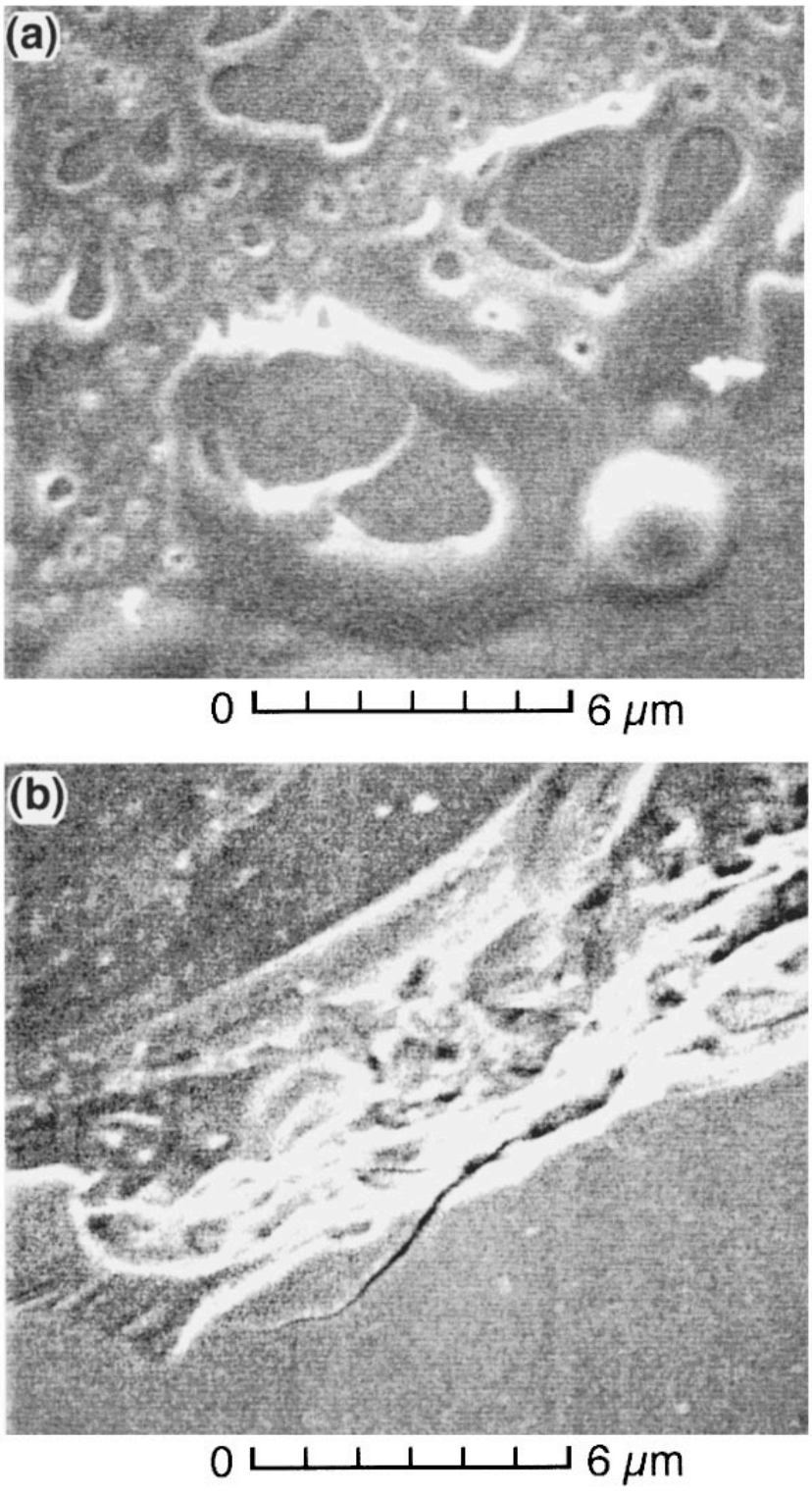

Figure 4.2 Edges of laser damage spots of Figure 4.1. (a) 900 picosecond pulse (b) 400 femtosecond pulse. (Stuart et al. 1996b)

Microscale laser damage and applications in micromachining

Although differences in damage for femtosecond and longer pulsed lasers are well documented in a number of studies (Du et al. 1994; Kautek et al. 1996; Stuart et al. 1995; Stuart et al. 1996b, 1996a; Varel et al. 1996), the first use of objective lenses for tight focusing of femtosecond pulses in order to manipulate material on the order of microns was performed by Glezer et al. (Glezer et al. 1996). Because of the highly nonlinear absorption, pulses can be focused within or through a transparent material using high numerical aperture lenses, allowing precise placement of 3-dimensional damage spots. Glezer et al. used bulk material modification by femtosecond laser pulses as a method for creating three-dimensional optical storage.

Later this work was extended to show that voids could be formed within the bulk of a material by focusing the laser within the material causing a micro-explosion that induced high-pressure shockwaves (Glezer and Mazur 1997; Juodkazis et al. 2006). Schaffer et al. then studied the effects of tightly focused laser pulses for the micromachining of structures by connecting multiple pulses to form waveguide structures (Schaffer et al. 2001) and the effects of different numerical aperture objective lenses on the morphology of the laser damage (Schaffer et al. 2004).

In 2003, A.P. Joglekar et al. published work that took advantage of the particular physical mechanisms for femtosecond laser damage to push laser machining to even smaller scales. Because of the highly nonlinear intensity dependence of damage, a sharp threshold above which damage occurs allows only a fraction of the Gaussian beam profile to cause ablation. This selection of a fraction of the beam allows the spatial extent of damage to be confined to a region less than the diffraction limited spot size. This damage can extend down to holes a few tens of nanometers in width, shown in Figure 4.3. This work removed material from the surface rather than performing bulk modification, however the same ability to string successive pulses together to form grooves was demonstrated (Joglekar et al. 2003; Joglekar et al. 2004).

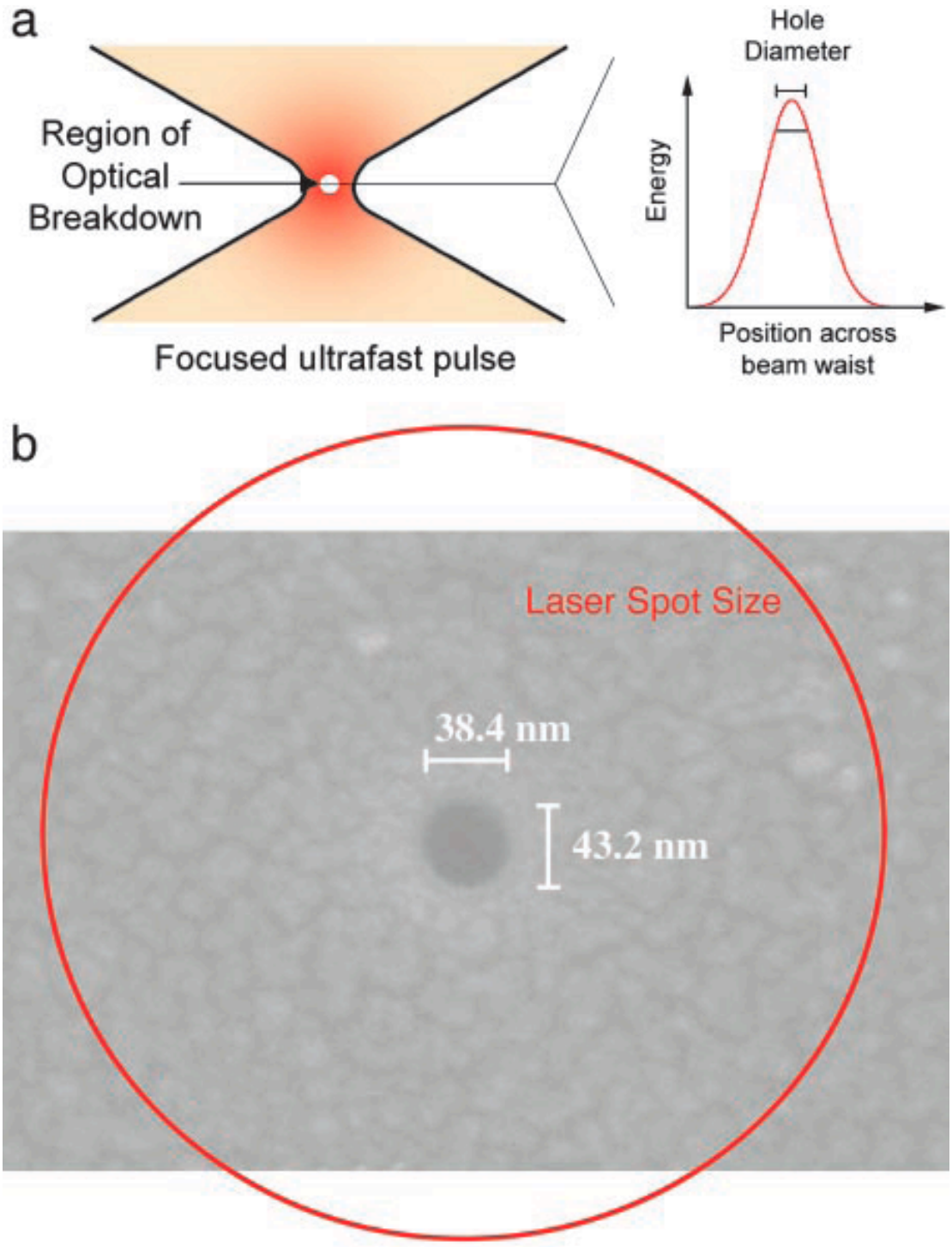

Figure 4.3 (a) An illustration of the technique used to machine sub-diffraction limited spot size holes in transparent dielectrics. (b) A scanning electron microscope image showing damage from a single, femtosecond duration pulse. The calculated spot size is shown as a red circle. (Joglekar et al. 2004)

It was also shown to be possible to machine complex three-dimensional structures in glass using water-assisted debris removal (Ke et al. 2005). As observed in Figure 4.4, this work shows that machined channels were smooth, regular, and highly circular in cross section.

Although this technique has been shown to be effective for machining on the micro and nanoscale, many questions remained regarding the physics of tightly focused laser damage. The following chapter, Chapter 5, discusses new physics and phenomena discovered for tightly focused laser damage as the pulse energy is increased above the damage threshold. The subsequent chapter, Chapter 6, examines the depth of holes formed by single pulses. Although the diameter of damage craters can be readily measured using a scanning electron microscope, information regarding the depth of these craters is not as easily accessible. This chapter discusses damage depth measurements and the discovery of the formation of nanochannels.

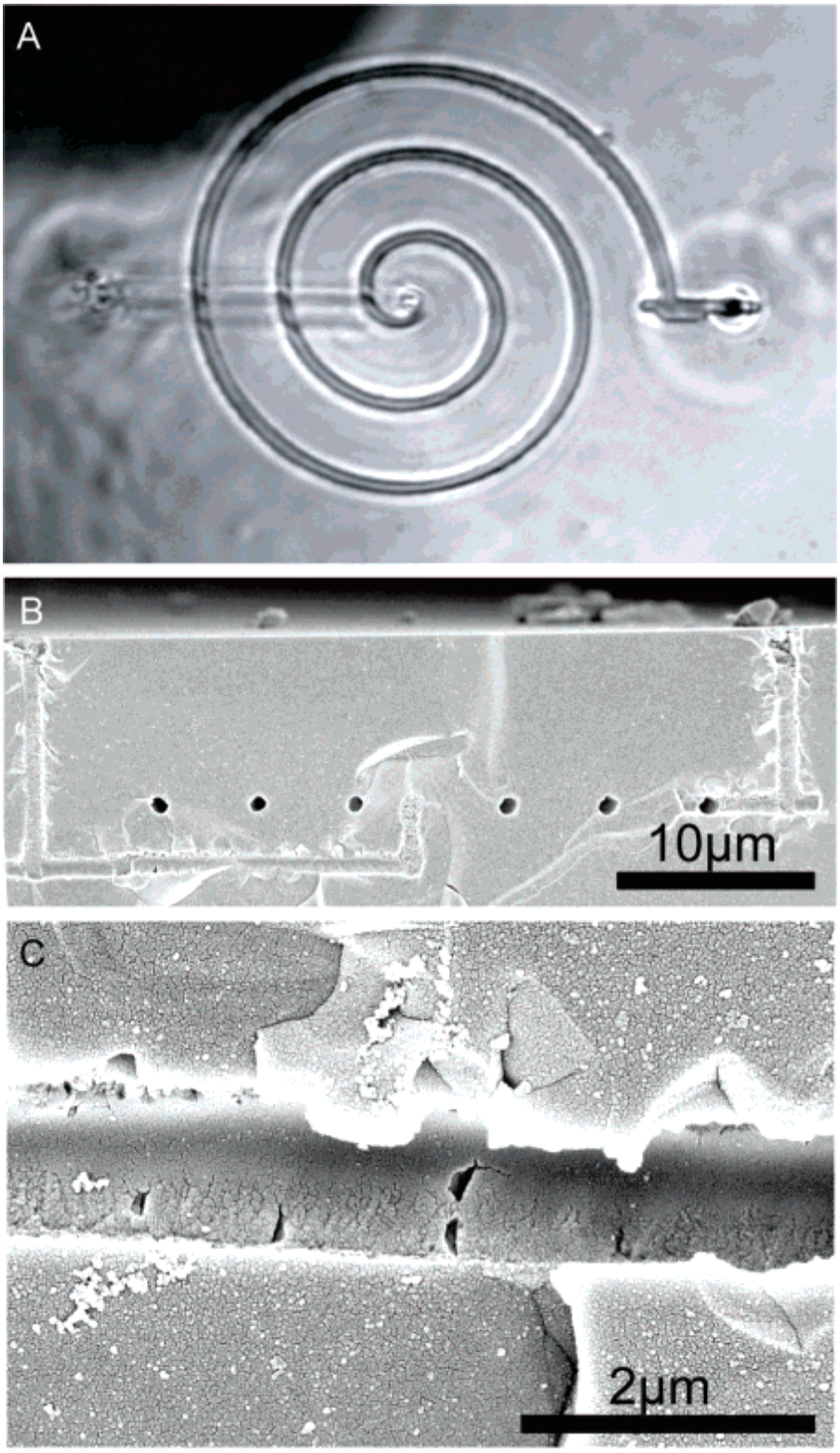

Figure 4.4 A Spiral channel machined in glass using femtosecond laser pulses. (a) Transmitted light image (b) Scanning electron microscope image of channel cross section. (c) Close up SEM image of the channel showing the surface roughness.

References

Du, D., et al. (1994), 'Laser-Induced Breakdown by Impact Ionization in Sio2 with Pulse Widths from 7 Ns to 150 Fs', *Applied Physics Letters,* 64 (23), 3071-73.

Glezer, E. N. and Mazur, E. (1997), 'Ultrafast-laser driven micro-explosions in transparent materials', *Applied Physics Letters,* 71 (7), 882-84.

Glezer, E. N., et al. (1996), 'Three-dimensional optical storage inside transparent materials', *Optics Letters,* 21 (24), 2023-25.

Joglekar, A. P., et al. (2004), 'Optics at critical intensity: Applications to nanomorphing', *Proceedings of the National Academy of Sciences of the United States of America,* 101 (16), 5856-61.

--- (2003), 'A study of the deterministic character of optical damage by femtosecond laser pulses and applications to nanomachining', *Applied Physics B-Lasers and Optics,* 77 (1), 25-30.

Juodkazis, S., et al. (2006), 'Laser-induced microexplosion confined in the bulk of a sapphire crystal: Evidence of multimegabar pressures', *Physical Review Letters,* 96 (16), 4.

Kautek, W., et al. (1996), 'Laser ablation of dielectrics with pulse durations between 20 fs and 3 ps', *Applied Physics Letters,* 69 (21), 3146-48.

Ke, K., Hasselbrink, E. F., and Hunt, A. J. (2005), 'Rapidly prototyped three-dimensional nanofluidic channel networks in glass substrates', *Analytical Chemistry,* 77 (16), 5083-88.

Kudryashov, S. I., et al. (2007), 'Nanochannels fabricated by high-intensity femtosecond laser pulses on dielectric surfaces', *Applied Physics Letters,* 91.

Pronko, P. P., et al. (1995), 'MACHINING OF SUBMICRON HOLES USING A FEMTOSECOND LASER AT 800-NM', *Optics Communications,* 114 (1-2), 106-10.

Scaffidi, J., et al. (2003), 'Dual-pulse laser-induced breakdown spectroscopy with combinations of femtosecond and nanosecond laser pulses', *Applied Optics,* 42 (30), 6099-106.

Schaffer, C. B., Jamison, A. O., and Mazur, E. (2004), 'Morphology of femtosecond laser-induced structural changes in bulk transparent materials', *Applied Physics Letters,* 84 (9), 1441-43.

Schaffer, C. B., et al. (2001), 'Micromachining bulk glass by use of femtosecond laser pulses with nanojoule energy', *Optics Letters,* 26 (2), 93-95.

Stuart, B. C., et al. (1995), 'Laser-Induced Damage in Dielectrics with Nanosecond to Subpicosecond Pulses', *Physical Review Letters,* 74 (12), 2248-51.

--- (1996a), 'Optical ablation by high-power short-pulse lasers', *Journal of the Optical Society of America B-Optical Physics,* 13 (2), 459-68.

--- (1996b), 'Nanosecond-to-femtosecond laser-induced breakdown in dielectrics', *Physical Review B,* 53 (4), 1749-61.

Varel, H., et al. (1996), 'Laser-induced damage in SiO2 and CaF2 with picosecond and femtosecond laser pulses', *Applied Physics a-Materials Science & Processing,* 62 (3), 293-94.

Chapter 5

Microscale grommet formation for tightly focused femtosecond laser damage at glass surfaces

Note: Major portions of this chapter are sourced from the article *Morphologies and non-linear scaling of laser damage on glass surfaces by tightly focused femtosecond pulses.* J.F. Herbstman, A.J. Hunt and S.M. Yalisove. Applied Physics Letters. **93** (2008).

This chapter extends work discussed previously by Joglekar et al. studying femtosecond laser damage at high numerical aperture and examines the relationship between pulse energy and the morphology of damage by a femtosecond pulsed laser, tightly-focused onto the back surface of glass. For fluences up to three times that of threshold, an unexpected discontinuity in the scaling of damage size is caused by ejection of rings of material surrounding central damage that appear above a sharp threshold fluence. A mechanism for the production of these structures via thermal expansion and shockwave generation is proposed.

A discontinuity in the relationship between damage diameter and fluence is present in width measurements of damage, corresponding to a change in the morphology of the damage, when a laser is focused by a 0.65 NA objective lens through a Corning 0211 glass coverslip to the back surface. As the fluence increases past the discontinuity, the commonly considered damage mechanism of thermal vaporization is augmented by the ejection of grommet-shaped features. Characterization of the formation of these “grommets" is performed and mechanisms for their origin are discussed.

Experimental Setup

A 600 fs directly diode pumped Nd:glass CPA laser (Intralase Corp., Irvine, CA) was frequency doubled using a KTP crystal to generate 527 nm light. Single pulses were selected using a shutter and attenuated using a neutral density filter wheel. A polarizing cube or λ/4 waveplate was inserted in the beam path to respectively linearly or circularly polarize the light. The beam was then sent into an inverted microscope and focused using microscope objectives of different numerical apertures (NA) with the back aperture of each objective filled with light to obtain the full NA. The laser was focused at a glass-water interface on the far side of Corning 0211 glass coverslips (Fisher Scientific, Waltham, MA) placed on a three-axis nanopositioning stage (Mad City Labs Inc. Madison, WI). Once damaged, the samples were coated with carbon and examined with a scanning electron microscope (FEI Nova Nanolab, Hillsboro, OR) at the University of Michigan Electron Microbeam Analysis Laboratory.

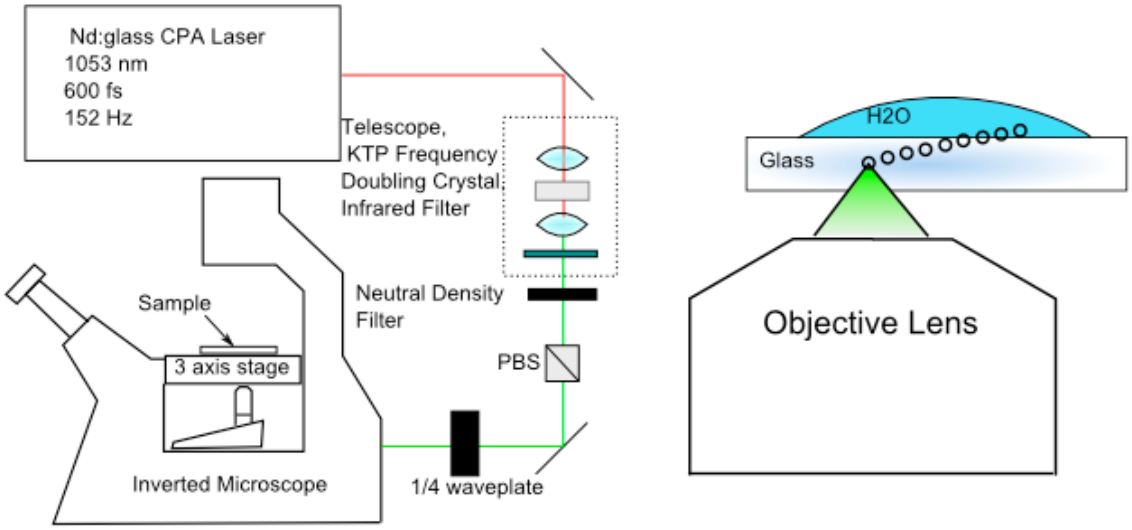

Figure 5.1. (Left) Experimental setup schematic for laser damage study. (Right) Close-up of the laser interaction with the glass. Each successive pulse is focused on a different location and a different depth in the sample.

Single pulses were fired at undamaged regions while making small changes in the height of the focus relative to the surface of the sample. The resulting central hole is to first approximation presumed to be largest where the focus and the surface coincide. The relation between diameter and fluence was fit to the inverse of a Gaussian curve, with the diameter, $D = \sigma (\ln(I/\gamma))^{1/2}$, where I is the peak pulse fluence, σ and γ are fitting parameters, with γ giving the damage threshold, corresponding to the fluence where this curve predicts zero diameter damage (Joglekar et al. 2003).

As shown in Figure 5.2, when the laser was focused with an 0.65 NA objective, a clear discontinuity in the size of the damage feature occurs at ~30 J/cm^2, below which sizes are dramatically reduced. As observed in previous work (Joglekar et al. 2003; Joglekar et al. 2004; Kudryashov et al. 2007), damage consists of a deep central hole, surrounded by a region of variable morphology. In contrast to the entire feature, the central hole size smoothly decreases with fluence, and the curve can be extrapolated down to the threshold for damage. The break in the curve describing feature size indicates an abrupt shift to a different damage mechanism, and closer examination of the damage spots reveals striking differences in the damage morphologies below and above the fluence at which the discontinuity occurs.

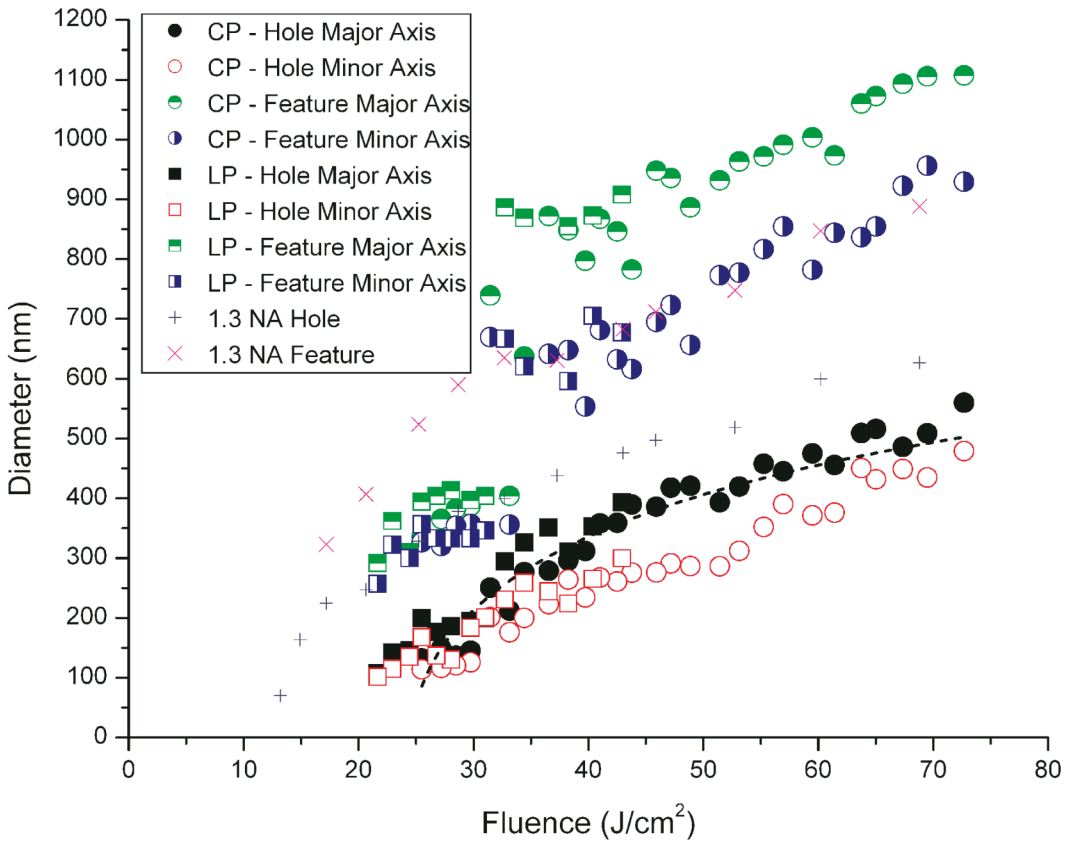

Figure 5.2 Damage in Corning 0211 glass for light that is circularly polarized (CP) at 0.65 NA and linearly polarized (LP) at 0.65 NA and 1.3 NA focusing conditions. Because of an elliptical beam shape, both the major and minor axes were measured for 0.65 NA, while damage for 1.3 NA did not display ellipticity. A line was fitted using the equation $D = \sigma (\ln(I/\gamma))^{1/2}$ to the data for the central holes for 0.65 NA.

Damage observed at fluences close to threshold below the discontinuity exhibit a smooth central hole and raised outer ring, shown in Figure 5.3(b). This damage is broadly similar to that seen in previous published work (Joglekar et al. 2003), but also exhibits small bumps on the raised outer ring; this may be because, unlike the previous work, damage occurs at a water-glass interface. The presence of water at the damage site rapidly quenches heated material, potentially preventing the material forming the small bumps from being extruded entirely, as seen in previously described spallation occurring for damage at a glass-air interface (Kudryashov et al. 2007). The morphology of damage at fluences above the size discontinuity, illustrated in Figure 5.3(c), is markedly different.

The clean central hole is still present, but a thinner, flat, grommet-like structure is ejected from the surrounding material for both glass-air and glass-water interfaces. However, in the presence of water, for fluences near the size discontinuity, the grommets sometimes remain partially attached to the substrate (Figure 5.4(a) and (b)). The grommets have a relatively flat bottom, conical sidewalls, and a small lip near the surface of the glass. These details can be observed in Figures 5.4 and 5.5. At a higher NA of 0.80, one can observe similar damage morphology (seen in Figure 5.4(c)) with removal of a central hole and an outer ring of material. Neither grommets nor removal of an outer ring of material were observed under tighter focusing conditions using a 1.3 NA objective. This phenomenon was also absent when the laser was focused at the near surface of the coverslip using a 0.65 NA objective.

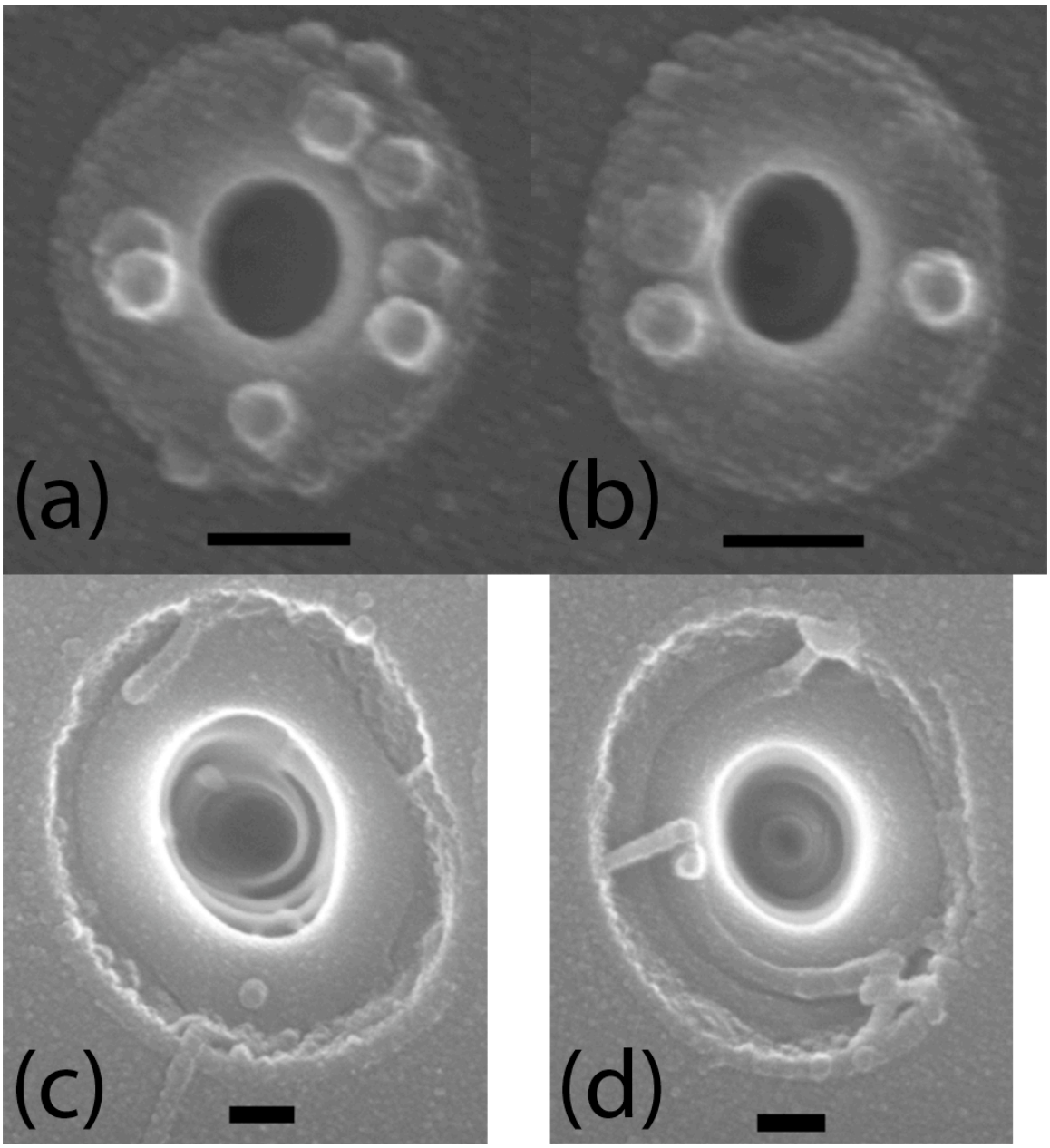

Figure 5.3 Top down SEM images of 0.65 NA damage in Corning 0211 glass. (a) CP 23 J/cm^2, (b) LP 23 J/cm^2 (c) 55 J/cm^2 (d) 43 J/cm^2. Scale bar length on all images is 100 nm.

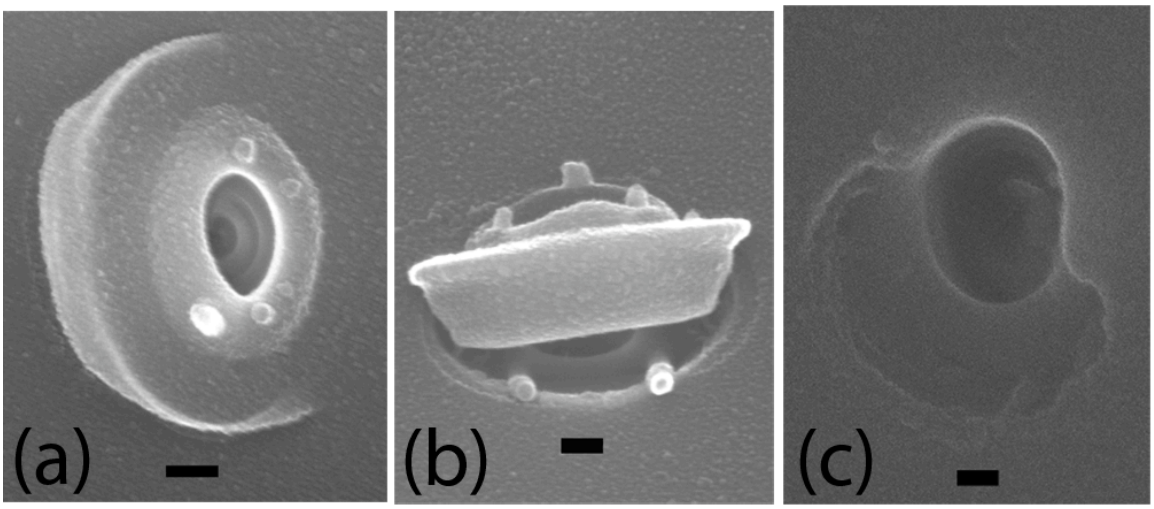

Figure 5.4 (a) 0.65 NA, LP, 40 J/cm^2. (b) 0.65 NA, LP, 34 J/cm^2. Image taken 30° from the orthogonal to the surface – this shows a profile view of the grommet, with the flat bottom, conical side and lip at the surface. (c) 0.80 NA, LP, 16 J/cm^2. Scale bar length is 100 nm.

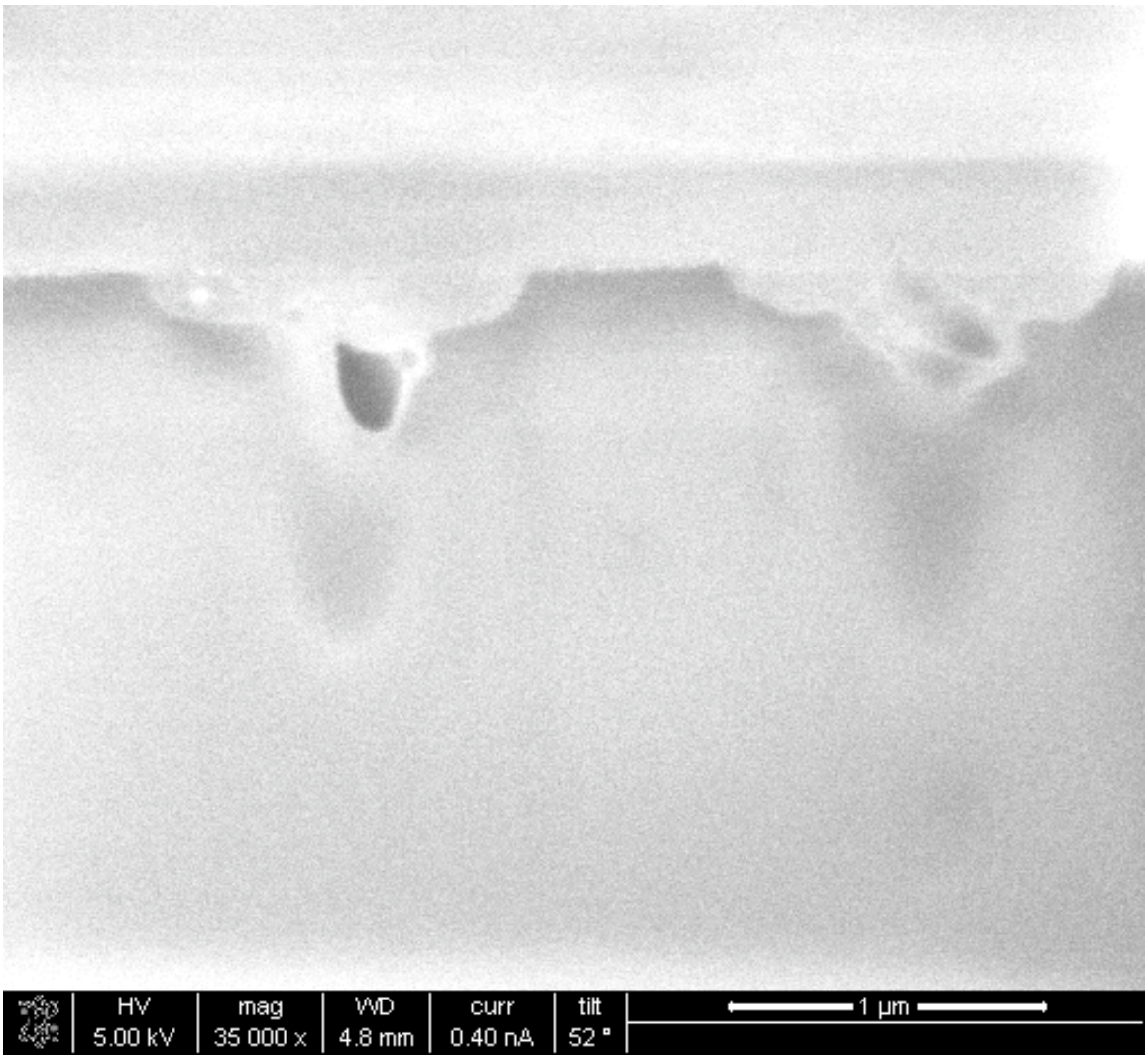

Figure 5.5 SEM images of grommet removal after the cross section is exposed using a Focused Ion Beam. The depth of removed material is ~200 nm.

The reproducible complexity of these features is intriguing, and the question arises as to how they are generated in a homogeneous, transparent solid. Where the laser comes to a focus at the back surface of the coverslip, an electron-hole plasma is generated via photoionization of carriers in the glass in regions where the intensity exceeds the sharp, highly non-linear threshold for damage (Bloembergen .N 1974; Tien et al. 1999). The excited carriers then thermalize, transferring their energy to the lattice: this causes superheating of the glass, leading to ablation of the material (Schaffer et al. 2001). The sharp, well-defined central hole formed at the fluences and NA examined is suggestive of

this type of ablation, characterized by heating and vaporization, with additional possible contributions from self-focusing (further addressed in the following chapter)(Kudryashov et al. 2007; Tien et al. 1999).

In Figure 5.6(a) & (c) the tilt-view perspective reveals thread-like structures projecting perpendicularly from the sample surface in the region surrounding the central holes. The thread-like structures seen in this figure indicate that a liquid phase of glass was created along with the central hole during damage. These threads, 30-60 nm in diameter and less than ~1μm long and absent for damage at a glass-air surface, likely occur when jets of molten material erupting from the central hole are quenched by the water at the glass surface. Near the damage threshold, blister-like structures (Figure 5.6(c) and (d)) are formed when the focus is slightly sub-surface. Similar blistering has been transiently observed in metals during femtosecond laser ablation and explained by the formation of a layer of two-phase gas and liquid material that expands away from the layer of non ablated material below the skin depth (Sokolowski-Tinten et al. 1998), but this has not previously been observed in a homogeneous, transparent dielectric. The blister-like structures that we observe suggest a similar mechanism occurs in glass under focusing conditions that cause a deposition of energy within a small depth range (Schaffer et al. 2004). As energy is absorbed, the temperature increases and vacancies generated by heating become more mobile. Simulations (in metals) show that these vacancies coalesce to form large voids in the material, while still leaving the surface layer intact (Leveugle et al. 2004). Rapid heating of the sub-surface absorption region leads to thermal expansion and generation of a shockwave that pushes the surface of the glass outward, creating a bubble of two-phase gas and molten material (Kudryashov et al. 2007; Leveugle et al. 2004; Sokolowski-Tinten et al. 1998). Figure 5.7 provides an illustration of this process.

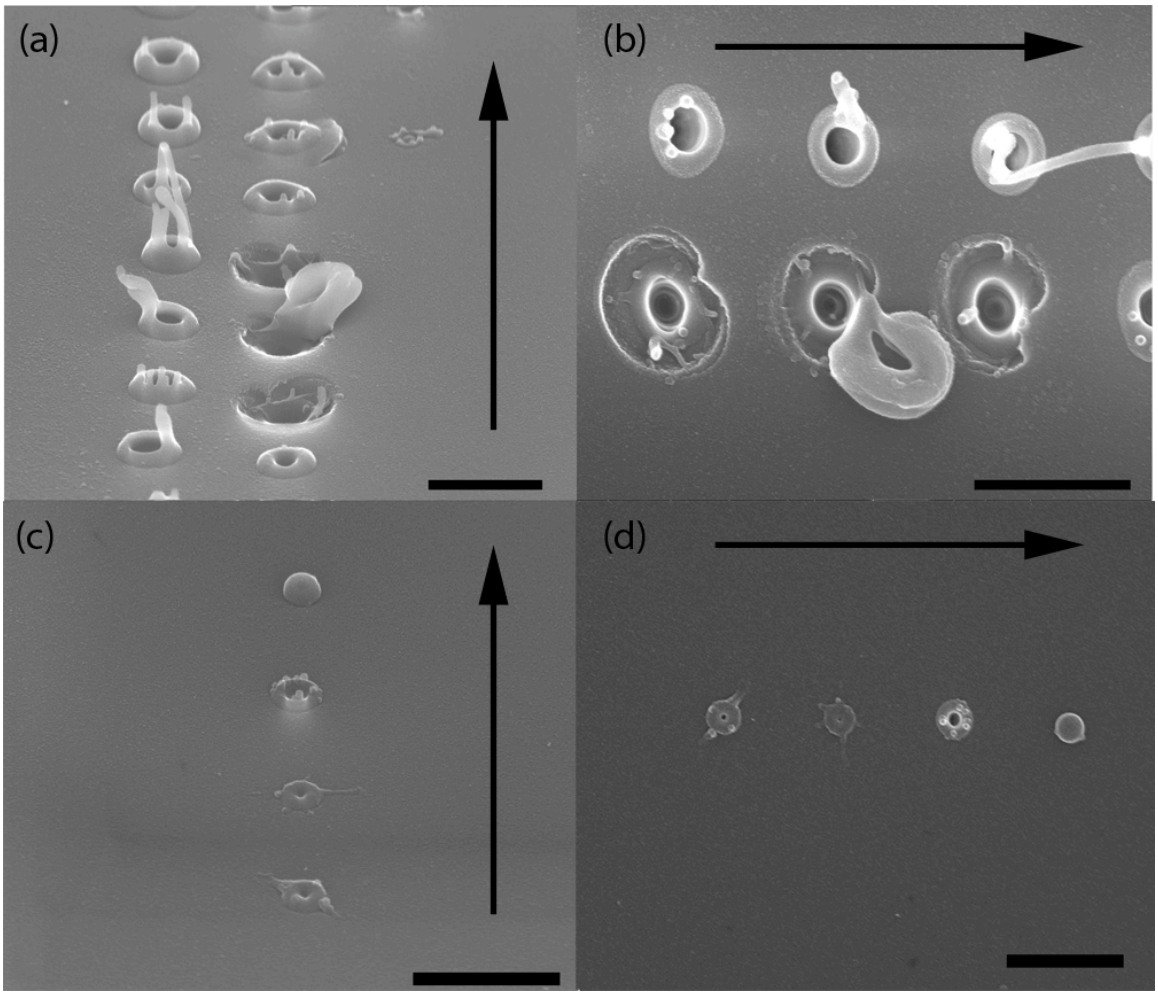

Figure 5.6 (a) Side view and (b) Top view images of 40 J/cm^2 damage. (d) Side view and (d) Top view images of damage near threshold (23 J/cm^2). The laser is focused deeper inside the glass surface for each spot in the direction that the arrows indicate, thus in (c) the top holes are focused deeper below the surface. In (a) and (b) the right/bottom row of damage occurs when the focus is near the surface, while the left/top row is focused deeper inside the material. The focus is scanned through the surface so that measurements of the damage threshold can be taken as close to the beam waist as possible. Images on the right side are taken orthogonally to the surface, images on the left side are taken at 55(a) and 47 (c) degrees from the orthogonal. Scale Bar is 1 μm.

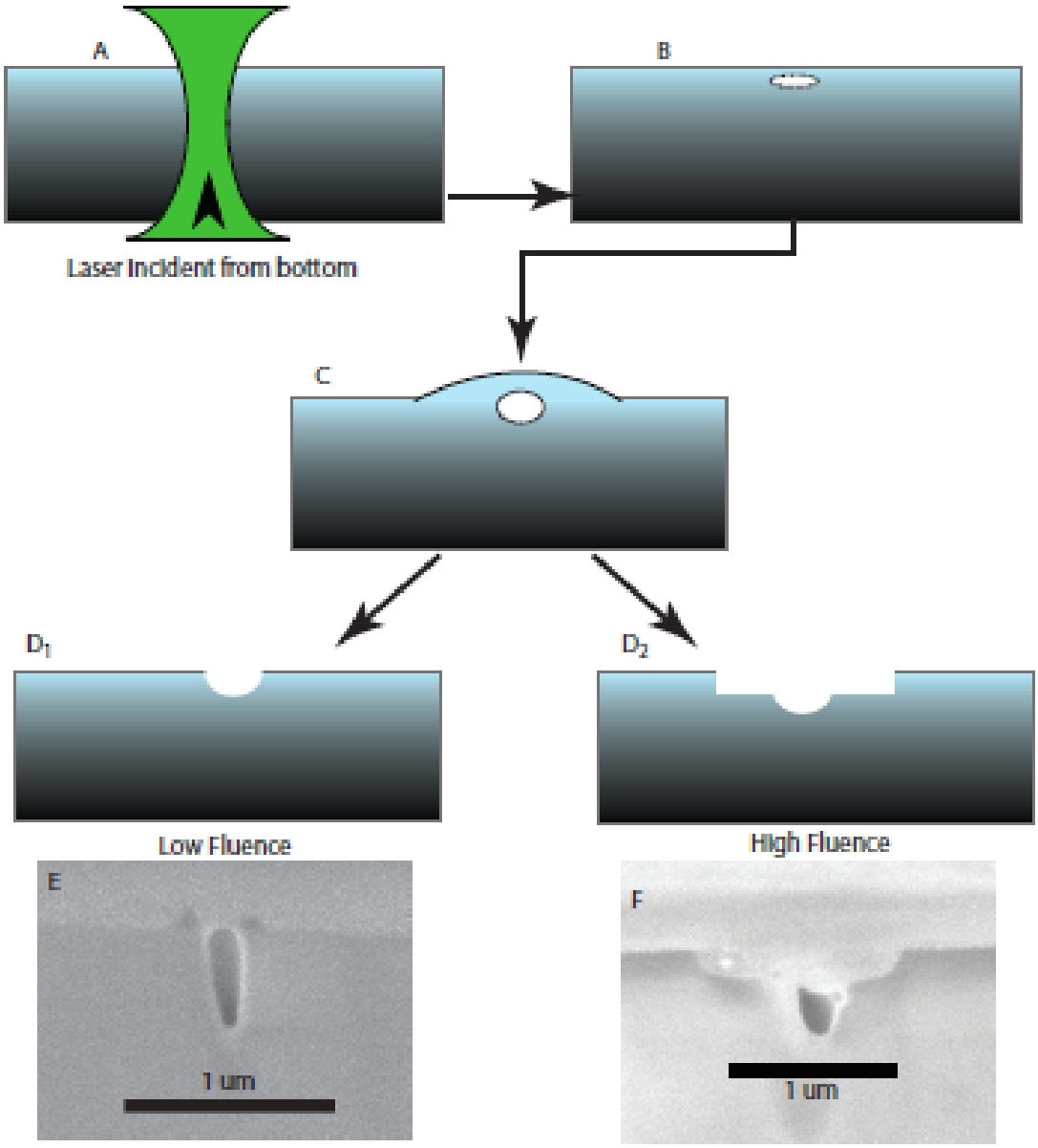

Figure 5.7 Cartoon illustration of the damage process. As the laser pulse passes through the sample (A), nonlinear absorption occurs. As the ionized electrons begin interacting with the lattice, energy is transferred to the ions. As the defects in the lattice coalesce into voids (B) the material is heated. The resulting absorbing region expands (C) and if near the surface, is ablated and ejected into the covering medium (D_1). At high fluences, the subsurface absorption and subsequent shockwave can remove the surface layer completely, as in the grommet removal process described above (D_2). FIB cross sections (E),(F) of these images support this theory.

The grommets ejected at fluences above the size discontinuity have not been previously observed. These grommets are less deformed than the glass threads described above, suggesting they are below melting temperature when ejected, and are formed through a different process than the vaporization that produces the central holes. For damage fluences well above threshold, heavy absorption and damage at greater depth is expected as ionization occurs upstream of the focal region (Schaffer et al. 2004). Thus when the beam waist is located at the surface, subsurface energy absorption will cause expansion both radially into areas with less deposited energy, and orthogonally to the surface, pushing the surface of the material outward, causing ejection of a solid layer if the deposited energy is sufficient to exceed the fracture strength of the glass. As seen in Figure 5.3(c) & (d), for fluences twice that of threshold, the gigapascal pressures that have been observed for tightly focused ultrafast damage (Kudryashov et al. 2008, McDoanld et al. 2008) can be large enough to totally remove the grommet. As the fluence is lowered, the grommet layer is not entirely removed, forming an attached structure as seen in Figures 5.4 (a) & (b) and 5.6(a) & (b).

Grommet ejection was observed when the laser was focused with 0.65 and 0.80 NA objectives, but not for front surface damage nor with a 1.3 NA objective. This is consistent with subsurface absorption driving grommet ejection, as the larger Rayleigh lengths of the lower NA and backside focusing conditions allows energy to be deposited deeper below the surface focus, both in absolute terms and with respect to the beam waist. This subsurface energy deposition facilitates blister and subsequent grommet formation.

Additionally, the comparison of damage by linearly and circularly polarized light indicates that for the conditions tested, 0.65, 0.80 and 1.3 NA (only 0.65 shown here), there is no difference in threshold or morphology of damage. This extends, but is consistent with, experimental observations of Joglekar et al. (Joglekar et al. 2003) and contrasts with a difference in threshold for circular and linear polarizations at shorter pulse durations (Temnov et al. 2006). As pointed out by Temnov et al. these behaviors

support theoretical calculations by Kaiser et al. (Kaiser et al. 2000), predicting that at longer fs pulse duration there should be little difference in damage thresholds.

In conclusion, while damage near threshold at the surface of glass produces sharp, sub-diffraction limit holes, at marginally higher fluences the damage features become complex. At fluences below the size discontinuity marking the onset of grommet formation, subsurface energy absorption can generate blister-like structures. As the fluence increases, increasing energy is absorbed upstream of the beam focus at the surface, and grommet shaped chunks are created due to shockwave formation. As incident pulse energy is increased, these subsurface shockwaves cause the surface layer to be ejected, generating a corresponding ring of removed material around the central hole. These findings show that for fs-laser damage in dielectrics, as the fluence is raised beyond threshold, energy dissipation processes quickly increase in complexity, and are central to determining the final damage morphology.

References:

Bloembergen .N (1974), 'Laser-Induced Electric Breakdown in Solids', *Ieee Journal of Quantum Electronics Qe10,* (3), 375-86.

Joglekar, A. P., et al. (2004), 'Optics at critical intensity: Applications to nanomorphing', *Proceedings of the National Academy of Sciences of the United States of America,* 101 (16), 5856-61.

--- (2003), 'A study of the deterministic character of optical damage by femtosecond laser pulses and applications to nanomachining', *Applied Physics B-Lasers and Optics,* 77 (1), 25-30.

Kaiser, A., et al. (2000), 'Microscopic processes in dielectrics under irradiation by subpicosecond laser pulses', *Physical Review B,* 61 (17), 11437-50.

Kudryashov, S. I., et al. (2007), 'Nanochannels fabricated by high-intensity femtosecond laser pulses on dielectric surfaces', *Applied Physics Letters,* 91.

--- (2008), 'Acoustic monitoring of microplasma formation and filamentation of tightly focused femtosecond laser pulses in silica glass', *Applied Physics Letters,* 92 (10).

Leveugle, E., Ivanov, D. S., and Zhigilei, L. V. (2004), 'Photomechanical spallation of molecular and metal targets: molecular dynamics study', *Applied Physics a-Materials Science & Processing,* 79 (7), 1643-55.

McDonald, J. P., et al. (2008), 'Femtosecond pulsed laser ablation dynamics and ablation morphology of nickel based superalloy CMSX-4', *Journal of Applied Physics,* 103 (9).

Schaffer, C. B., Brodeur, A., and Mazur, E. (2001), 'Laser-induced breakdown and damage in bulk transparent materials induced by tightly focused femtosecond laser pulses', *Measurement Science & Technology,* 12 (11), 1784-94.

Schaffer, C. B., Jamison, A. O., and Mazur, E. (2004), 'Morphology of femtosecond laser-induced structural changes in bulk transparent materials', *Applied Physics Letters,* 84 (9), 1441-43.

Sokolowski-Tinten, K., et al. (1998), 'Transient states of matter during short pulse laser ablation', *Physical Review Letters,* 81 (1), 224-27.

Temnov, V. V., et al. (2006), 'Multiphoton ionization in dielectrics: Comparison of circular and linear polarization', *Physical Review Letters,* 97 (23), Art.

Tien, A. C., et al. (1999), 'Short-pulse laser damage in transparent materials as a function of pulse duration', *Physical Review Letters,* 82 (19), 3883-86.

Chapter 6

Nanochannel formation in glass produced by tightly focused, single femtosecond laser pulses

Note: Portions of this chapter are sourced from the articles:

Nanochannels fabricated by high-intensity femtosecond laser pulses on dielectric surfaces. S.I. Kudryashov, et al. Applied Physics Letters **91** (2007).

High aspect-ratio nanochannel formation by single femtosecond laser pulses. J.F. Herbstman and A.J. Hunt. Optics Express **18** (2010).

Although the scaling and morphology of surface features for tightly focused femtosecond laser damage has been well documented (Herbstman et al. 2008; Joglekar et al. 2003; Schaffer et al. 2004), submicron damage provides a challenge for depth measurements. These holes are too small for accurate probing with optical techniques such as laser profilometry and geometry prevents an atomic force microscope (AFM) tip from fully probing the depth of the central hole without artifacts from crater walls. This section discusses techniques used to measure the depth of damage caused by single, tightly focused, femtosecond laser pulses. These techniques reveal that damage can extend a surprising distance into the target, forming nanochannels of lengths well beyond the dimensions of the laser focus. This chapter presents evidence that these channels are formed by nonlinear phenomena such as self-focusing and filamentation. Finally, this type of damage is ideal for a number of micromachining applications in that they allow high aspect-ratio channels to be created at high speeds. A number of applications are discussed.

Preliminary work by A.P. Joglekar investigating tightly focused femtosecond laser damage demonstrated that regular holes could be machined in glass at diameters well below the diffraction limited spot size (Joglekar et al. 2004). However the depth of this damage was unknown and not easily measured using standard top-down SEM techniques. Atomic force microscopy (AFM) is an excellent technique for measuring surface profiles

at this size scale, however because of expected effects and artifacts from tip interactions with the side walls of the damage crater, depth measurements using this method are unreliable. Laser profilometry can be used to probe surface structure but cannot probe dimensions of sub-wavelength damage with the correct precision.

The structure of this damage during machining was illuminated by Ke et al., as illustrated in Figure 6.1, when a microfluidic structure was cleaved, showing that the cross section of machined channels is circular (Ke et al. 2005). This shape is puzzling, as the calculated intensity profile at the focus is in the shape of a prolate spheroid, similar to the shape of a football. However, this profile is not observed in Figure 6.1, the channels appear to have a circular cross section.

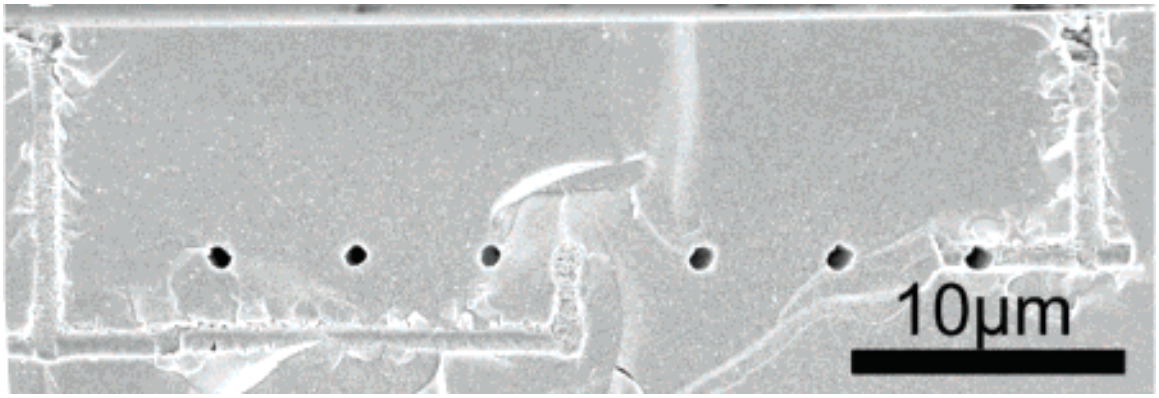

Figure 6.1 A cross section of a spiral channel obtained by cleaving the sample. From Ke et al., 2005. The machined channel shows a circular shape.

Further investigation of the cross section and depth of single pulse damage was carried out by using a simple procedure to cleave the sample along a damage crater. A diamond scribe was used to engrave a line across the sample with a small gap in the center. In this gap, a grid of holes was machined. The sample was then cleaved along the scribed line and placed in the SEM so that the cleaved surface was exposed and holes that aligned along the cleavage plane could be imaged in cross-section. This technique, shown in Figure 6.2, was successful in demonstrating that damage can extend several hundred nanometers into the bulk of the target, beyond the theoretical confocal parameter of the focusing optics of 529 nm. This confocal parameter, *b*, is twice the Rayleigh range and

can be estimated by the equation $b = 2\lambda/(n\pi(NA)^2)$.

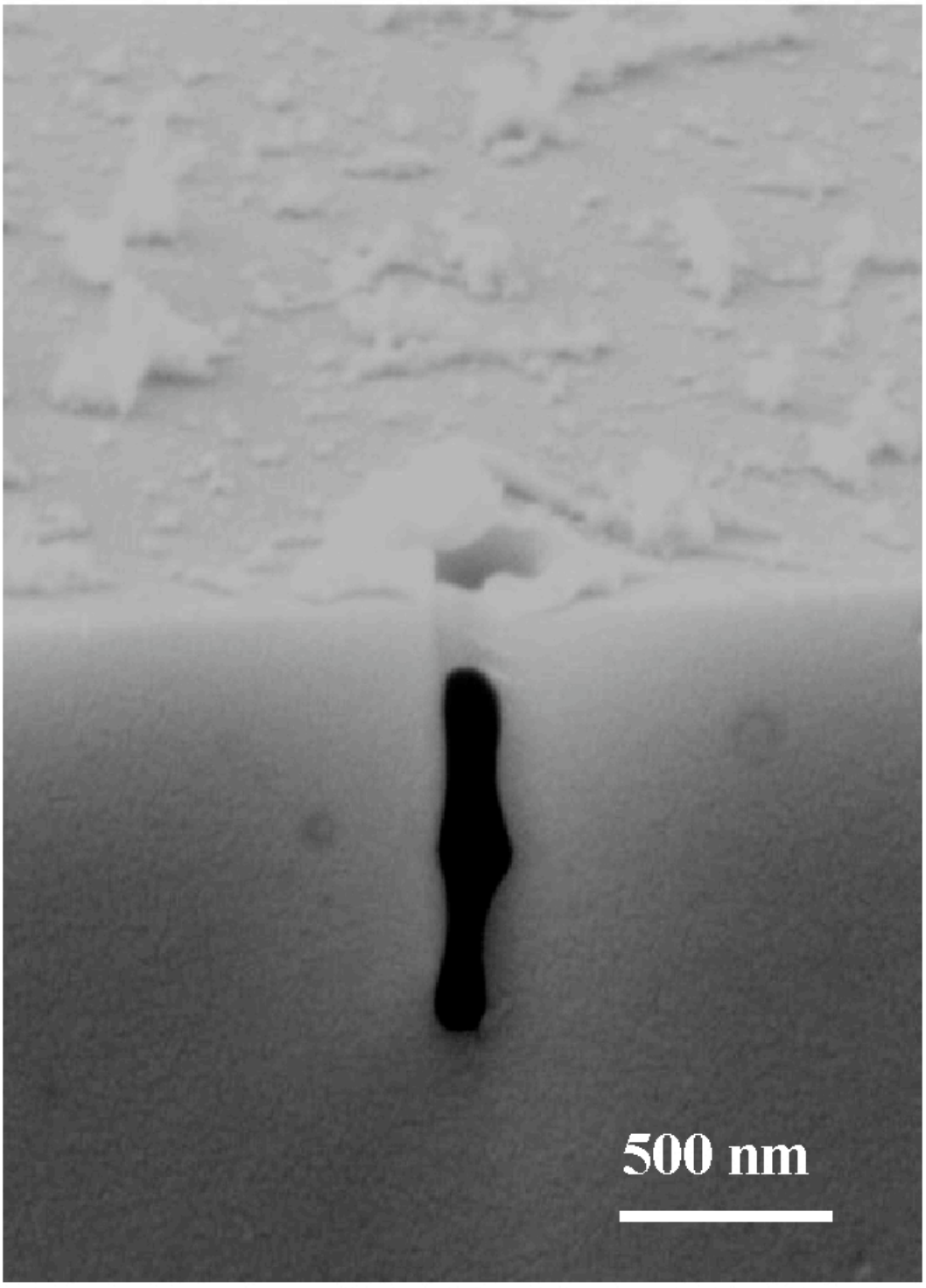

Figure 6.2 A Nanochannel formation in glass from damage at an intensity of 500 TW/cm^2. This channel was exposed via the cleavage method.

The discovery of damage that extended to this depth indicates that a mechanism allowed energy deposition effectively along the axial direction while still confining damage radially. A number of possible mechanisms for this behavior were suggested including: Bremsstrahlung X-ray generation and drilling, spherical aberration, and self-focusing (Kudryashov et al. 2007; White et al. 2008). Bremsstrahlung X-ray emission occurs when electrons are ionized and rapidly gain energy from the incident photons. These electrons then emit high frequency photons (X-rays) in a characteristic spectrum as they interact with ions from the material. This mechanism requires a hot (100 eV) absorbing surface layer of plasma emitting primarily in the forward direction that heats and melts the material along the axial direction.

Another possible mechanism for the elongated damage would be aberration effects, i.e. spherical aberration of the laser beam generating a focal region that is longer than would be expected. Although this form of aberration cannot be eliminated, objective lenses that focus the light can compensate to a large degree for this effect. Finally, nanochannels may be the result of nonlinear effects including self-focusing and filamentation. These effects would serve to refocus and elongate the region above the critical intensity for damage in glass.

To elucidate the mechanism for the production of nanochannels further study of the channels was required. Although the previously described technique for cleaving samples was successful in showing the depth of a single hole, it was a difficult method to control and had a number of disadvantages: it provided no ability to select which hole would be exposed, it did not ensure that cleavage that was flat and bisected the damage, and only small numbers of holes could be examined for each sample.

To improve the measurements of these nanochannels, additional techniques were required. First, samples were damaged using a similar experimental setup as was previously described. A Nd:glass laser (Intralase Corp., Irvine, CA) outputting 600 fs

pulses at a wavelength of 1053 nm and a repetition rate of 150 Hz was focused into a KTP frequency doubling crystal. The infrared light was filtered out and single 527 nm pulses were selected using a shutter. The beam was brought into the epifluorescence light path of an inverted microscope and focused using the 0.65 NA/40x Achroplan objective lens (Carl Zeiss, Inc., Thornwood, NY) allowing simultaneous imaging and damage. A nanopositioning stage (Mad City Labs Inc., Madison, WI) mounted on the microscope was used to manipulate Corning 0211 glass cover slips (Fisher Scientific, Waltham, MA) used as targets. The objective lens compensates for the spherical aberration caused by passing through the cover slip so that the tightest focus and minimal aberration is achieved at the rear coverglass surface. Conditions when the laser is focused through the cover slip to the rear surface are referred to as back side machining; front side machining refers to when the focus is at the near surface of the cover slip (Fig. 6.3a).

Samples were imaged using a Nova Nanolab DualBeam combined SEM and FIB (FEI Corp., Hillsboro, OR) at the University of Michigan Electron Microbeam Analysis Laboratory. After coating with ~4 nm of gold, the samples were placed in the electron microscope specimen chamber for imaging. The focused ion beam (FIB) was used to obtain cross sections of the laser damage by first coating the surface with a layer of platinum to protect the surface features, followed by FIB removal of the sample material until the full damage cross section was revealed (Fig. 6.3b).

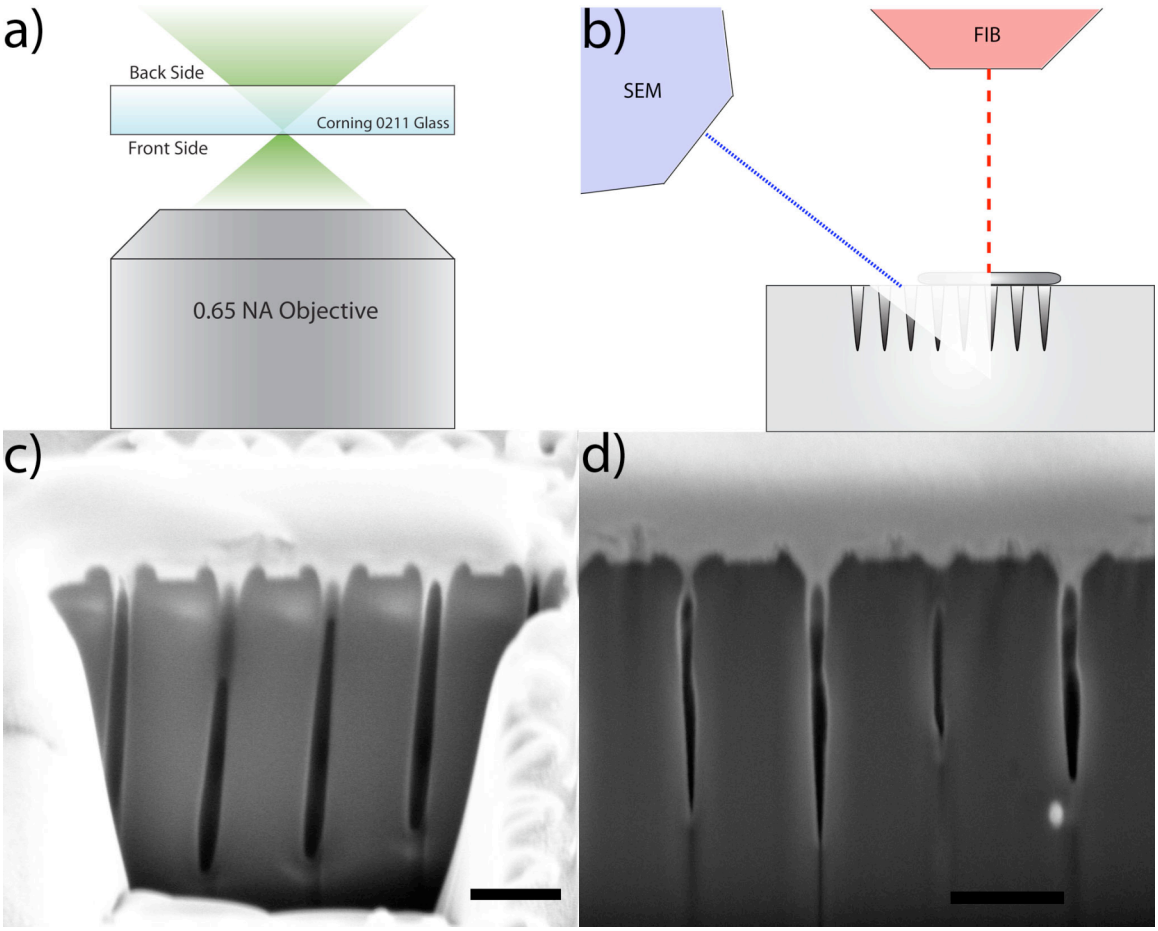

Figure 6.3 a) An illustration of the machining geometry, with the front and back side of the coverslip indicated. b) A damaged sample examined under a dual beam FIB/SEM. The FIB is placed perpendicular to the sample surface and the SEM is offset at a 52° angle. The sample is covered with a few hundred nanometers of platinum to protect the surface from unintended ion damage. The FIB removes a wedge from the sample, exposing the nanochannel cross-section. c) An example cross-section for back side machining. d) An example cross-section for front side machining. Both images show damage at 67 J/cm^2. Irregularities along the axial dimension of these channels are presumably the result of variations in FIB milling such that channels are not uniformly bisected. Scale bars indicate 1 μm.

Nanochannels are exposed in FIB cross sections of laser damage, allowing direct examination (Fig. 6.3). The channel profiles for both back and front side machining are shown in Fig. 6.3c and d respectively. In Fig. 6.3c, the longest channel is 4.06 μm deep and 240 nm wide; the longest channel in Fig. 6.33d is 3.12 μm by 157 nm. Under the optimal focusing conditions for the objective lens the confocal parameter has a length of

530 nm and a width at the beam waist of 344 nm. Thus these channels exhibit a void that is much longer than the calculated confocal parameter of the laser focus, and considerably smaller across than the diffraction limited beam waist. Additionally, one can observe a tapered profile extending into the material for channels fabricated using the front side technique, while those machined on the back side have a more rounded bottom (e.g. Fig 6.3c & d). Finally, these images show that channels are free from debris formed during the damage process. A small ring of melted and ejected material surrounds the channels, as previously observed (Joglekar et al. 2003; Kudryashov et al. 2007).

In order to quantify the morphology of a larger number of channels, acetate film surface replication was performed. This process melts a film onto the surface which, when removed, provides an imprint of the sample. The molten acetate flows freely into the nanoscale channels, allowing measurements of channel length across an array of channels. A back side machining acetate replica is shown in Fig. 6.4. This image shows replicas of the channels formed as the laser is focused progressively deeper into the bulk of the target. Most of the imprints stand perpendicularly off of the surface, while the deeper channel imprints sometimes topple and lay flat on the surface.

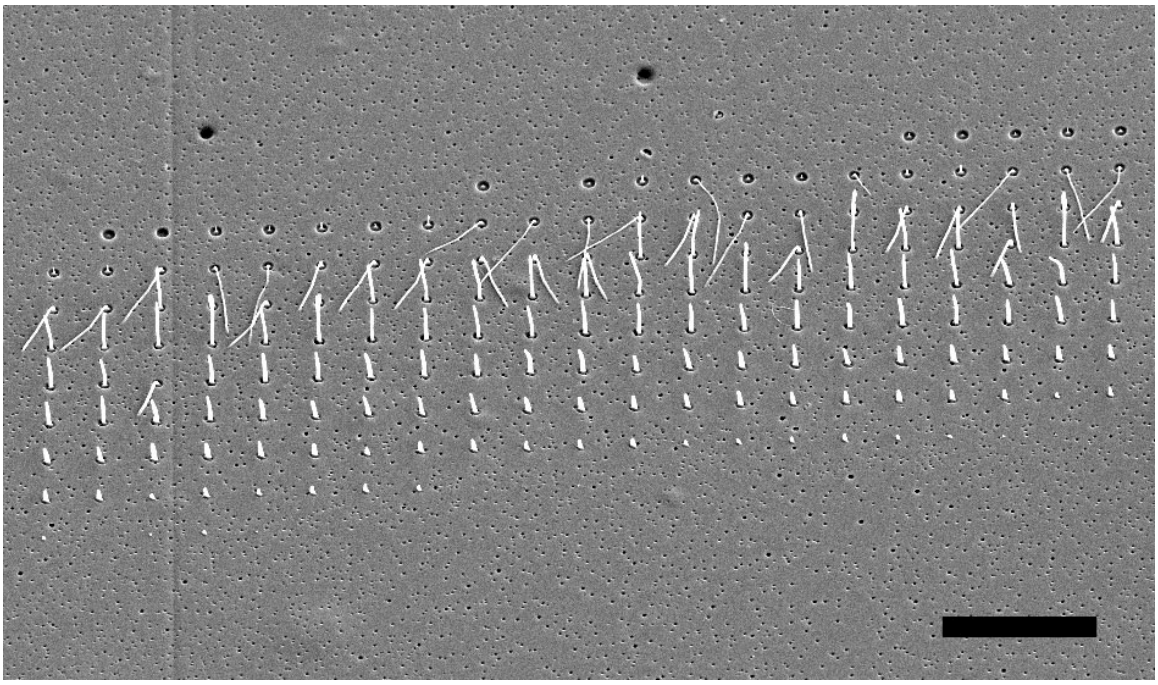

Figure 6.4 Back side machining sample showing single pulse laser damage at 74 J/cm^2 replicated using an acetate imprint. Pulses are focused 500 nm deeper with each row going from bottom to top in the vertical direction and 50 nm deeper with each pulse from right to left in the image. This image was taken at a sample tilt angle of 45°. The scale bar is 10 μm.

The length of the nanochannels increases as the laser focus moves deeper within the target. As shown in Fig. 6.5, the length of the channels increases in direct proportion with the depth of the laser focus: within the error the slope of a regression line is one, demonstrating a close correspondence between the focal depth and the channel length. This correspondence indicates that during channel formation material removal begins at a fixed point along the beam relative to the beam waist, such that the length of the channel is determined by the location of this point relative to the surface. This relation holds until the channels approach a point at which channels are either no longer formed, are resealed by melt, or they may become too thin to allow imprint replication (e.g. see upper imprints in Fig. 6.4).

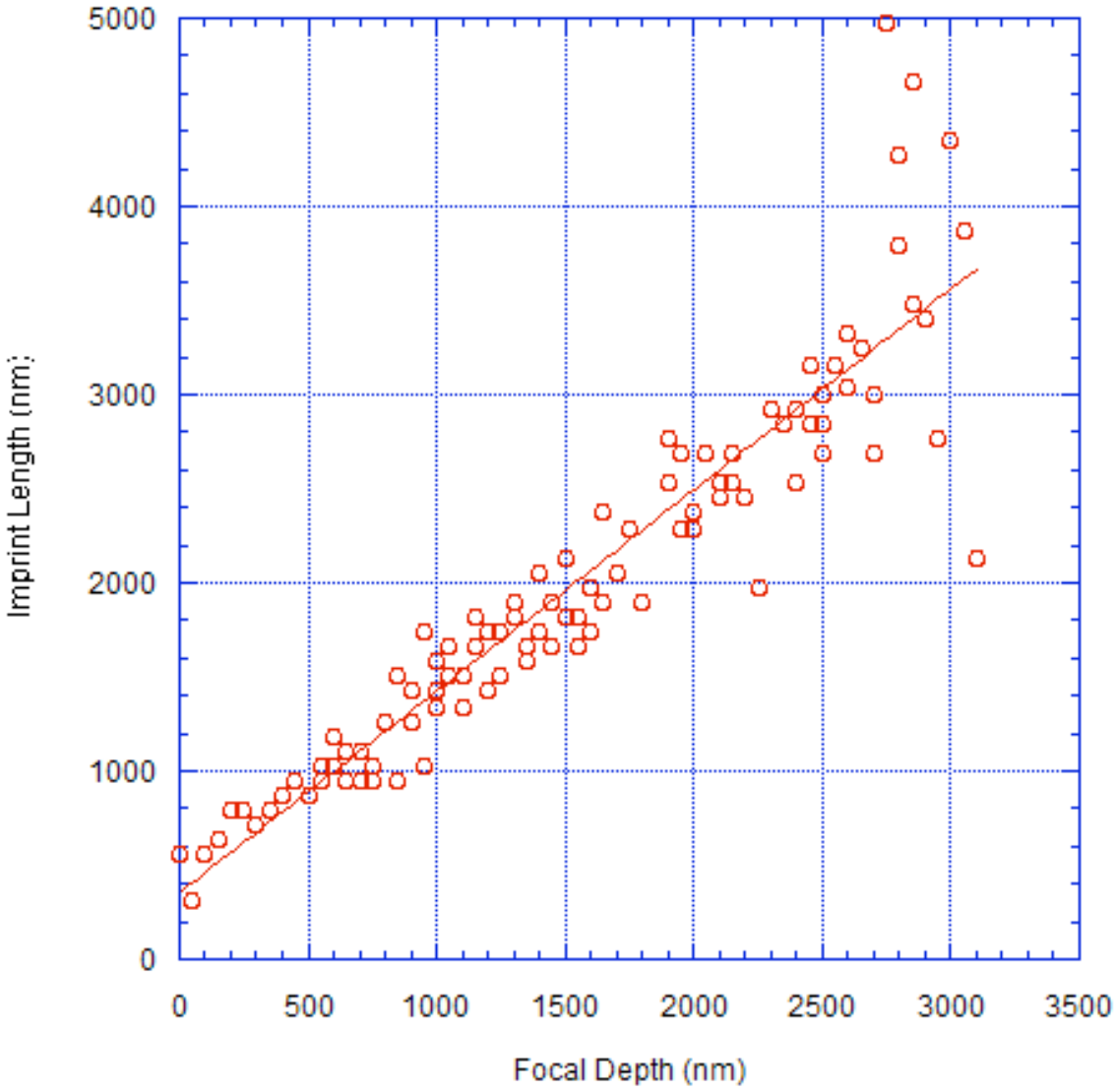

Figure 6.5 Back side machining sample measurements showing imprint length vs. focal depth, as measured from Figure 4. The least-squares regression line is plotted on the figure as a solid line. The slope of this line is 1.07±0.04. Because the precise location of the focus is difficult to determine with nanometer precision, the zero depth corresponds to the first observation of damage on the replica.

As shown in Fig. 6.6, the relationship between the maximum channel length and the fluence exhibits two behaviors. At pulse fluences below ~ 80 J/cm^2, the channel length increases with fluence up to about 8 μm; thereafter the curve plateaus such that further increases in fluence have less effect on the channel length. Across all fluences the

channel depth scales with the focal depth, with slopes for the regression lines fit to the data (e.g. Fig. 6.5) close to 1 (1.05±.04) as seen in Figure 6.7.

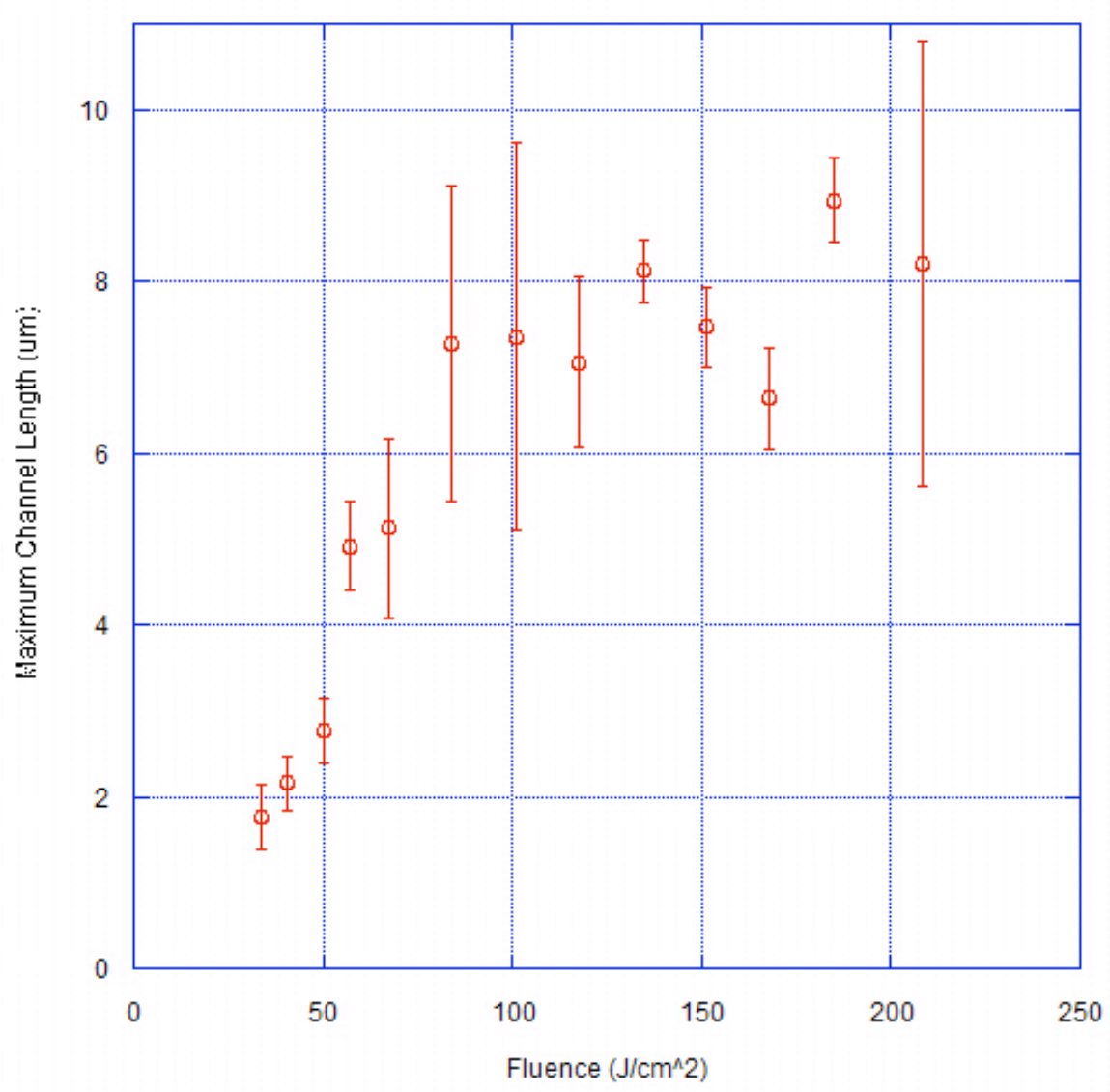

Figure 6.6 Back side machining sample measurements show that the maximum channel length increases with increasing fluence at low powers, but plateaus at ~8 µm for fluences above ~80 J/cm^2. The maximum channel length is obtained by taking the average of the four longest channels observed at each fluence.

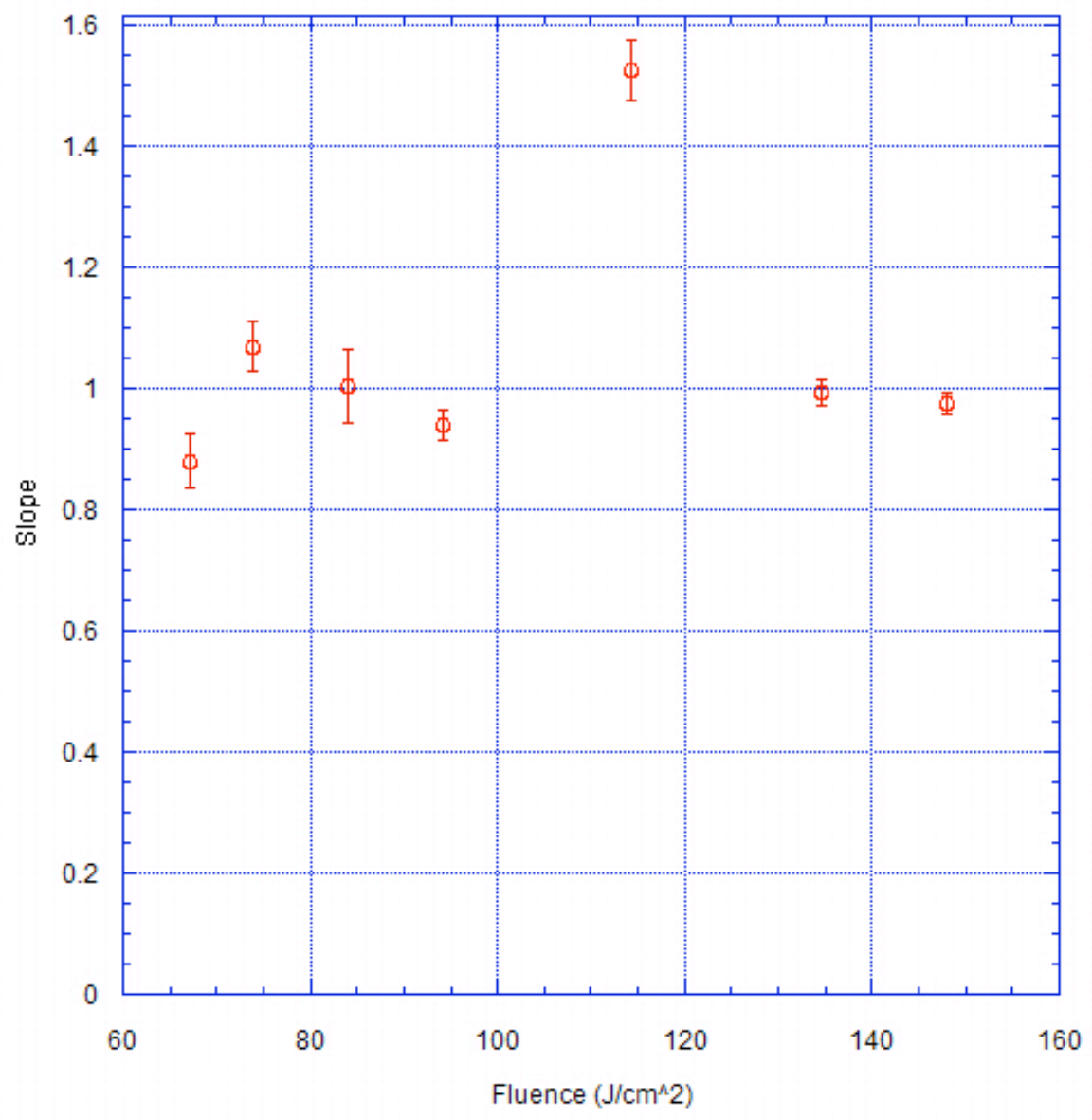

Figure 6.7 A plot of the slope of the regression line fitted to the channel length vs. focal depth for a range of fluences. The slopes are grouped near 1 (1.05±.04), with an outlier at 114 J/cm^2.

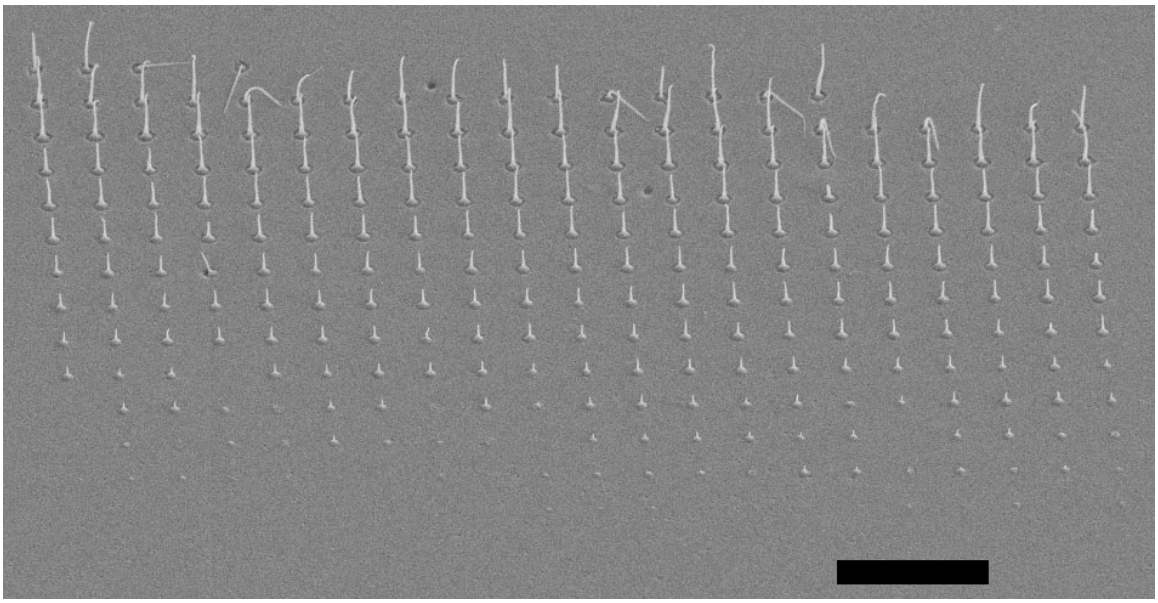

Figure 6.8 Front side machining damage at 118 J/cm^2 replicated using an acetate imprint. Pulses are focused 500 nm deeper with each row going from bottom to top in the vertical direction and 50 nm deeper with each pulse towards the right side of the image. This image was taken at a sample tilt angle of 45°. The scale bar is 10 μm.

Analysis of acetate replicas for front side machining similarly demonstrates that the channel length increases as the laser pulses are focused deeper into the glass. The tapering shape and thinner width of the front side channels is quite different than the more cylindrical shape of the channels formed during back side damage (Figs. 6.3d and 6.8). When the relationship between focal depth and channel length is examined, front side machining exhibits somewhat nonlinear scaling (Fig. 6.9). Additionally, as shown in Fig. 6.10, we observe that in contrast with back side machining the maximum channel length does not plateau; instead the length increases linearly with fluence across the

examined range.

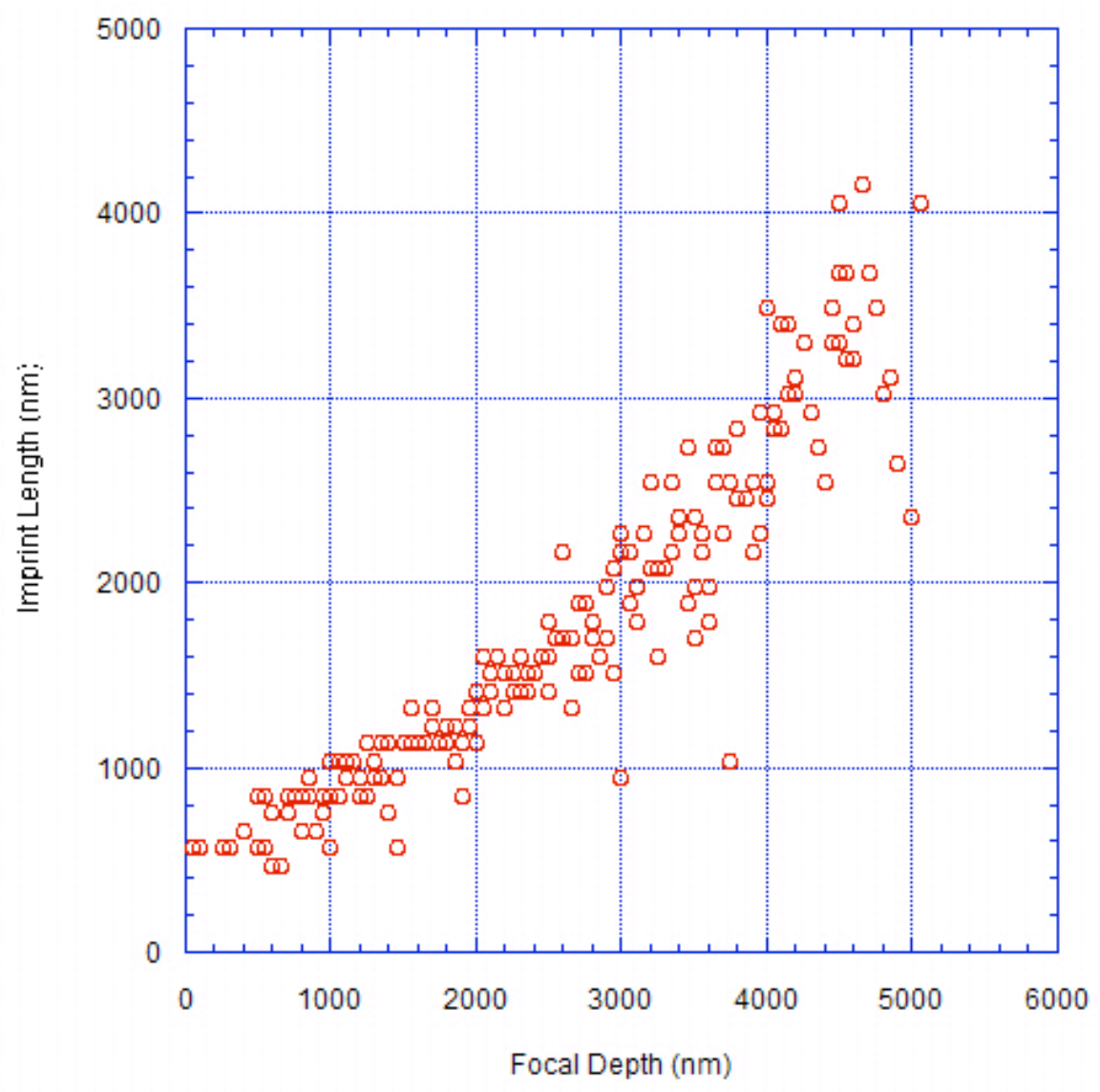

Figure 6.9 Front side machining imprint length vs. focal depth as measured from Figure 6.8 at 118 J/cm^2.

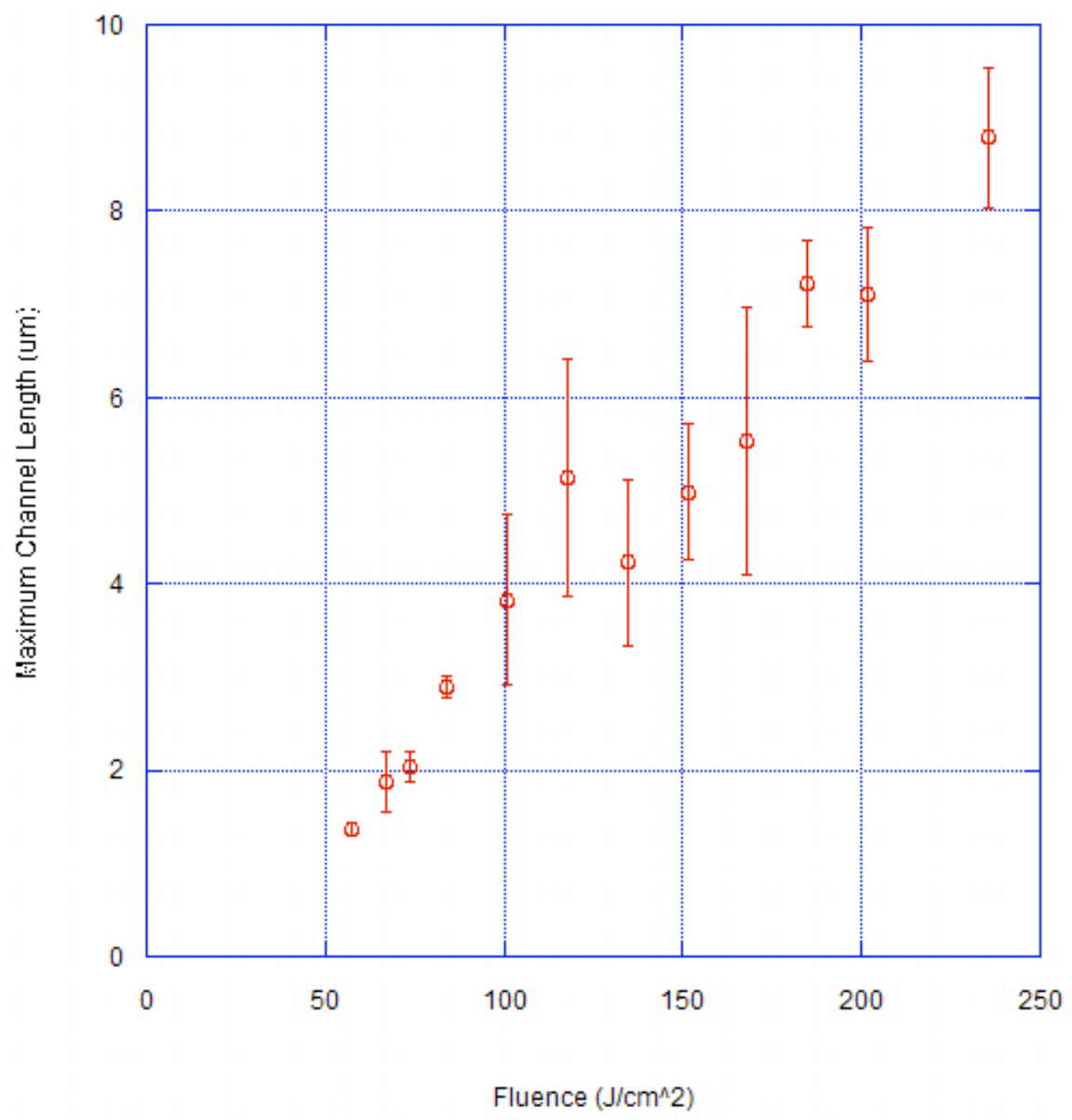

Figure 6.10 Front side machining maximum channel length vs. fluence. Maximum channel length is measured using the average of the four longest channels observed at each fluence.

These measurements demonstrate that for back side machining conditions, where spherical aberration is minimized, nanochannel formation occurs just as readily as in front side machining conditions, where substantial spherical aberration is expected. To quantify the degree of spherical aberration, we characterized the length of the focus using confocal microscopy at both the front and rear surfaces. This was accomplished by using the experimental objective lens to image with a confocal microscope and measuring the

spatial extent of emission along the z-axis from a sub-resolution fluorescent microsphere. The back side showed an estimated confocal parameter of 2.0 ± 0.1 μm, while the front side exhibited a confocal parameter of 4.2 ± 0.2 μm. Thus, while spherical aberration may affect the shape of the channel, it is not required for the extremely elongated morphology of the damage; indeed, the channels were generally longer for back side machining where spherical aberration is minimized (See Figs. 6 and 10).

A more general explanation for the formation of nanochannels in glass can be provided by nonlinear self-focusing and filamentation. Self-focusing will occur when, as the laser pulse begins interacting with the glass, the intensity of the pulse becomes large enough such that the linear approximation for the refractive index no longer holds. The pulse causes a dramatic increase in the refractive index of the material resulting in lens-like focusing of the beam. Additionally, as the beam begins to converge, it will cause ionization and form a plasma, serving to defocus the beam. The interplay between these two mechanisms can create an elongated region where the beam maintains a tight focus. The shapes of the nanochannels observed here through FIB cross section and acetate replication are consistent with the shape of previously observed laser filamentation damage tracks as well as calculated ionization profiles (Couairon et al. 2005).

Furthermore, both theoretical predictions and previous studies of femtosecond laser damage using multiple pulses (Couairon et al. 2005; Couairon and Mysyrowicz 2007; Schaffer et al. 2004; Shen 1984) incorporate self focusing and filamentation to show that with increasing pulse fluence the damage track will elongate and the initiation of damage will move upstream relative to the focus, as the converging beam reaches the critical fluence at an earlier position. The location relative to the focus where critical damage intensity is reached shifts upstream at most with the square root of the incident fluence. A larger extension of the damage track occurs due to continued ionization along the propagation axis from the self-focused laser pulse (Couairon et al. 2005). Consistent with this mechanism, for front side machining we observe a clear dependence of channel length on the incident pulse fluence (Fig. 6.10). The lengths of the nanochannels formed by back side machining show similar dependence on the laser fluence up to a plateau.

The plateau exhibited in Figure 6.4 may be the result of viscous resistance for extrusion of material, preventing clear channels above 8 μm in length, presenting the possibility of clearing longer channels with multiple pulses. The higher threshold for damage at the front side and limitations of the laser output prevent this plateau from being observed for front side damage. These results predict that a similar plateau would be observed for front side damage at higher fluences. Additionally, the effect of the increase in fluence may be mitigated by intensity clamping, where the balance of self-focusing and plasma defocusing set a limit on the peak intensity that occurs in the filament (Liu et al. 2002).

For back side damage at a particular fluence, the location at which critical fluence is reached and damage is initiated has homogeneous upstream conditions whether near the surface or several microns distant. Thus, the channel length depends only on the distance between the point where critical intensity is reached and the surface, up until this distance exceeds the maximum possible channel length, such that the surface is no longer breached, causing the linear dependence on the position of the focus. However, for front side machining the spot size of the focused beam on the glass surface where damage initiates depends on the position of focus relative to the surface. Thus the conditions where damage initiates change as the focus of the laser pulse is moved relative to the sample surface, creating conditions for a nonlinear extension of the channel presumably formed by laser filamentation seen in Figure 6.9. Furthermore, the generation of Bremsstrahlung x-rays can be eliminated as the source of damage due to the high directionality of the damage and clear dependence of channel length on the focal depth. At a particular fluence, one would expect very weak dependence on focal depth for x-ray drilling, as the highly energetic plasma that emits the x-rays would occur primarily on the surface and would not be dependent on the focus depth (Kudryashov et al. 2007).

The highly elongated damage formed by the 0.65 NA focusing conditions is also present under very high NA. Using a 1.3 NA objective lens, the focus should display a confocal parameter of ~130 nm, on the order of the beam spot size at the focus (~170 nm FWHM). Using FIB cross sections to image this damage, illustrated in Figure 6.11, we observe that nanochannels up to ~1.5 μm deep can be formed from single pulse damage. Although

capable of forming long channels, the damage that occurs when the pulse is focused at the surface is roughly circular and hemispherical. Successive pulses directed at the surface will form a circular cross section as this region is preferentially ablated to form channels.

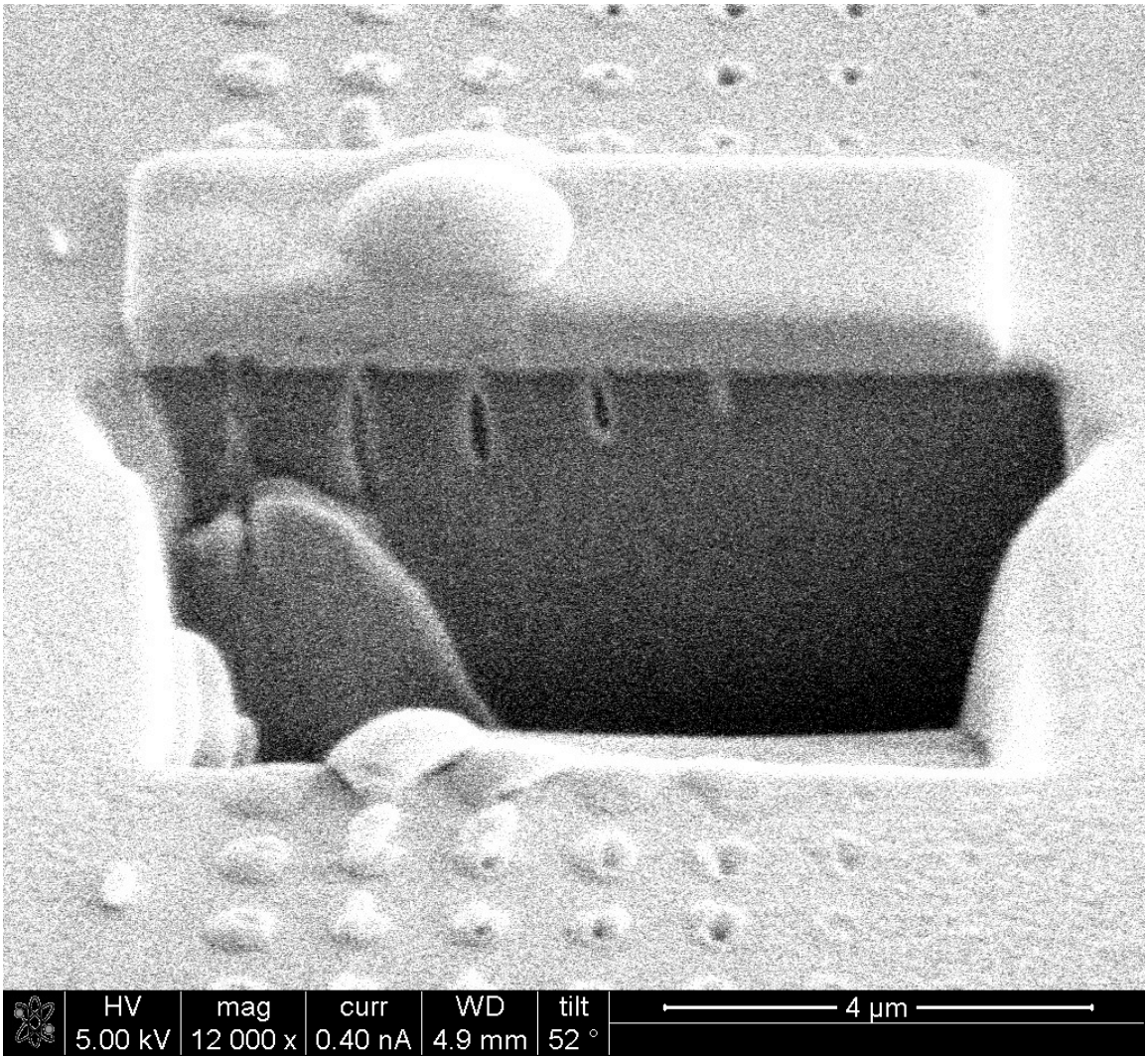

Figure 6.11 Nanochannel formation for 1.3 NA single pulse damage at 101 J/cm^2. The channel lengths from the right are 510, 780, 1080, and 1470 nm. The projection in the left side of the cross section is the result of milling irregularities along the exposed surface.

This elongation of femtosecond laser damage, strongly linked to filamentation, has a number of exciting potential applications. The ability to form channels with single pulses addresses one of the fundamental disadvantages for industrial applications of laser

machining; structures must be formed serially, rather than in parallel as with photolithographic techniques. With recent advances in laser technology allowing high repetition rate, high average power femtosecond lasers (Keller 2003), formation of long channels using single pulses could allow fabrication speeds as high as 400 m/s. Thus femtosecond laser machining would approach rates comparable to photolithographic techniques, while enabling nanoscale and three-dimensional features to be formed outside of a clean room. This allows a range of scientific and industrial applications. Including large arrays of nanowells, both in-plane and out-of-plane modification of patterned structures, 3-dimensional lithography performed entirely with a single optical machining device (McDonald et al. 2006a), and the high aspect ratio relaxes the requirements for nanoscale calibration between the laser focus and a surface when holes are drilled. The following section describes a number of preliminary structures machined using nanochannel phenomena.

Nanochannel Applications

The ability to pattern high-aspect ratio nanochannels with single pulses opens up a number of applications for nanomachining. These channels can be machined at very high speeds, approaching that of the repetition rate of the laser, allowing this micromanipulation technique to compete with photolithography for specialized applications. Some of the preliminary applications that have been pursued have included out-of-plane vias for optically patterned silicon oxide tube and regular arrays of nanowells.

One excellent example of a proven application for single pulse nanochannel formation is the creation of out-of-plane vias for silicon oxide tubes optically patterned on silicon. Previous work by J.P. McDonald et al. has shown that a femtosecond laser focused at the interface between a silicon substrate and a custom grown oxide layer can cause blister formation between these two layers (McDonald et al. 2006a; McDonald et al. 2006b). The blisters can be overlapped, allowing large tubes to be formed. This space created in

the gap between the layers can be used for microfluidic applications at a large range of size scales from micrometers up to centimeters. A potential use for these microfluidic structures might be to execute measurements of electrical and biochemical properties of individual cells. However, this application requires that the tubes be accessed with small, submicron pores. The single pulse nanochannel machining described above provides an excellent technique for accessing these tubes accurately, reliably, and quickly. Sample oxide tubes were patterned by R. Murphy in the Yalisove laboratory in the Materials Science Dept. of the University of Michigan. These samples were then machined using single and multiple pulses to fully access the interior of the tube. Figure 6.11 illustrates one submicron channel machined in the oxide layer of a tube sample. This pore is ~440 nm wide. Figure 6.12 shows a cross-section exposed using the FIB to illustrate that the channels penetrate fully to access the oxide tube.

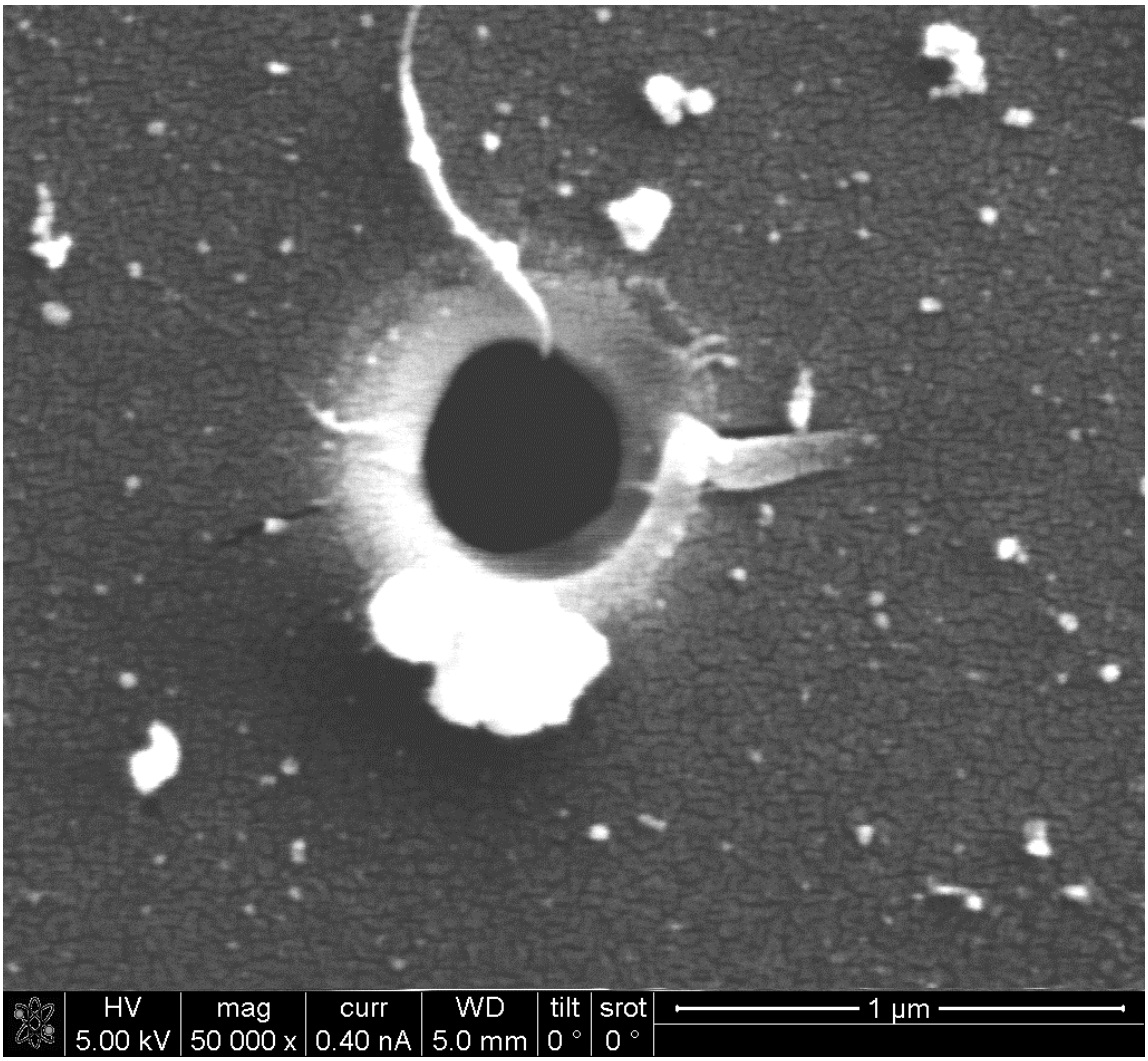

Figure 6.12 A hole created by a single pulse in a silicon/silicon dioxide tube. This pore is ~440 nm in diameter.

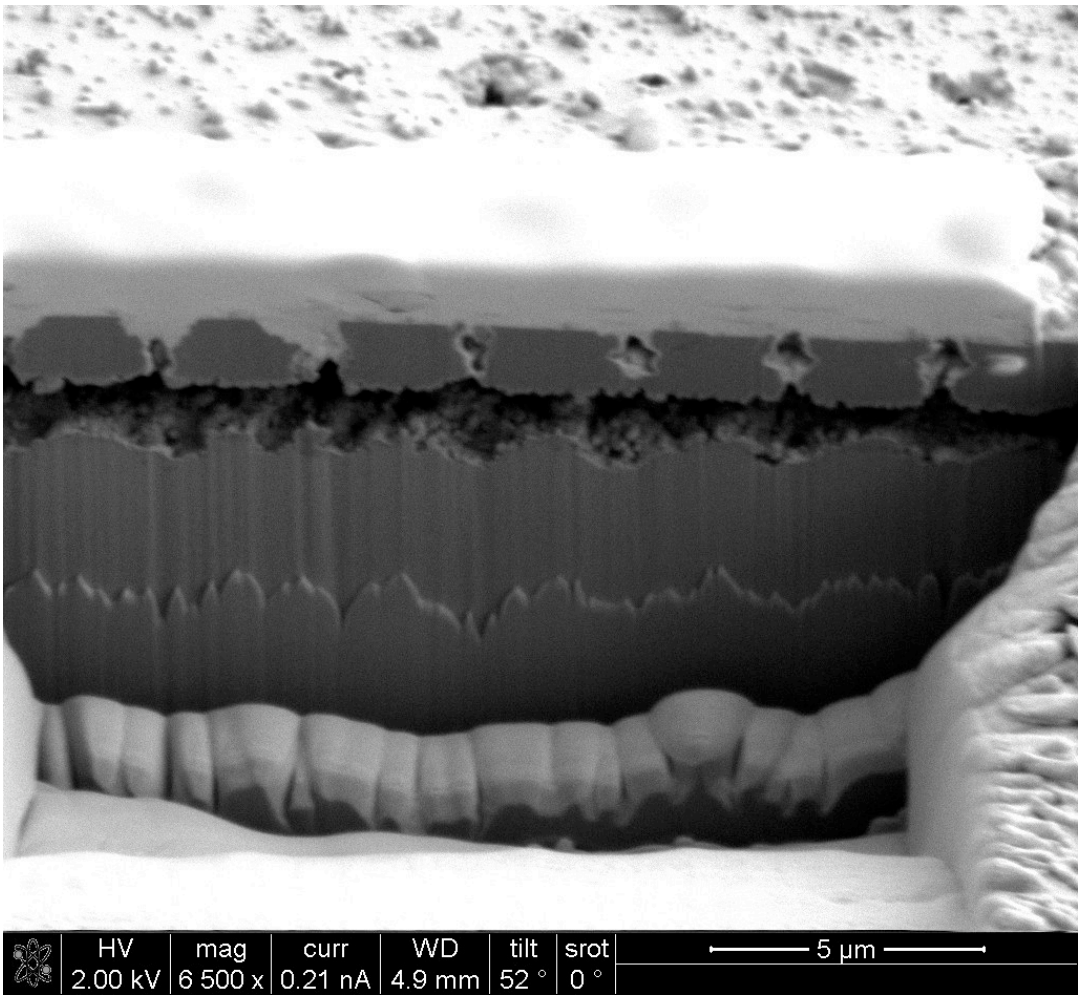

Figure 6.13 An FIB cross section showing that holes can be machined through the oxide layer. Here, the oxide layer is covered in a platinum to protect the surface during FIB milling. This platinum layer has a lighter contrast than the oxide layer beneath. The dark, bottom layer is the silicon substrate.

Experiments with single nanochannel vias drilled to access oxide tubes demonstrate that these tubes can successfully carry current when filled with a buffer solution. Figure 6.13 demonstrates a conductance measurement trial with a simple geometry, two access nanochannels on either end of an oxide tube. The channel was filled with Dulbecco's PBS buffer solution. This solution had a measured conductivity of 19 mS/cm at room temperature. Electrodes were placed on both ends of the tube and electrolytic flow was generated. The slope of this I-V curve shows a resistance for the channel of 285 MΩ. The expected resistance for a channel of similar dimensions, 1 cm long, 10 µm wide and

2 μm tall, or this buffer solution would be 260 MΩ. For reference, the access resistance for the nanochannels in this geometry is ~260 kΩ.

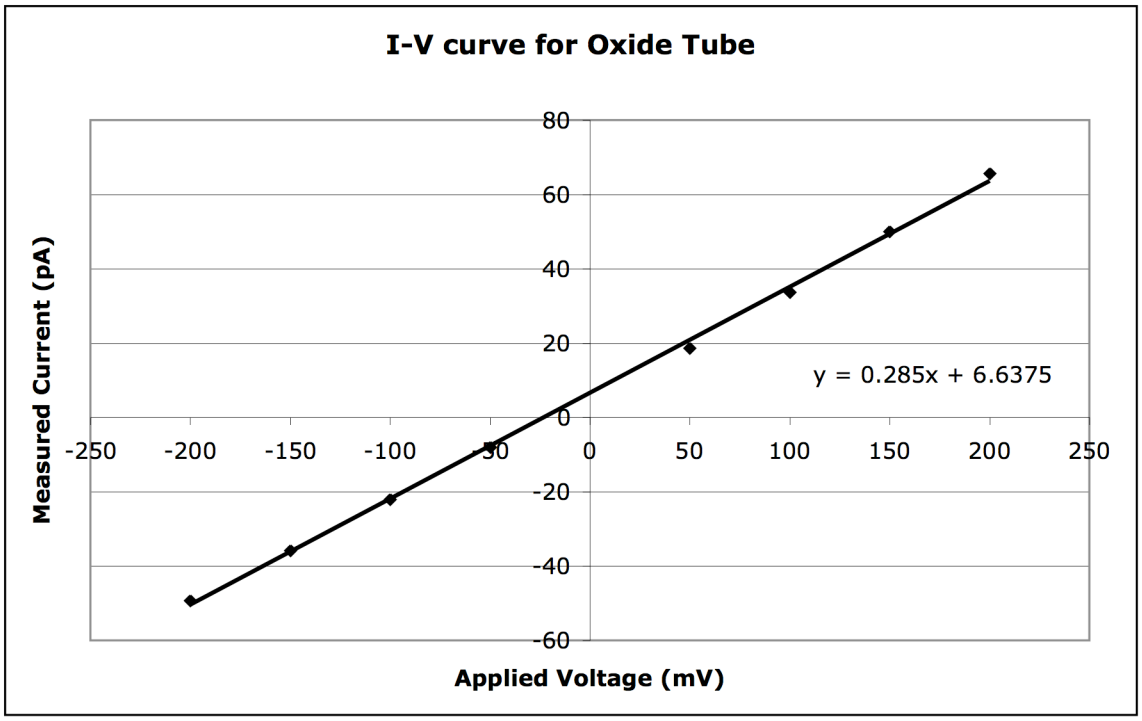

Figure 6.14 I-V curve for a Silicon Oxide tube accessed with nanochannels. The slope of the line fitted here indicates that the resistance of the tube is 285 MΩ.

Another application for experimental use is the fabrication of a regular array of channels to be used as extremely low volume wells (~10^{-19} m^3). Combining an array of these wells with confocal microscopy allows tracking of single molecule transport through a cellular pore or diffusion through a permeable membrane that can be placed over the array. The high aspect ratio of these wells is vital, in that it allows for an inspection volume deep below the surface that is removed from spurious surface signal. Figure 6.13 illustrates an imprint of an example well array fabricated using back side machining. Figure 6.14 shows an array of wells formed by front side machining. These wells have a different shape and lower volume than those for back side machining.

These applications are a few of the many novel and interesting ways that these channels can be utilized for microfluidic applications. A number of future potential applications

are available to be pursued including the machining of nanopores, precision crack initiation for fracture study, and integrated micro-optical Bragg reflectors.

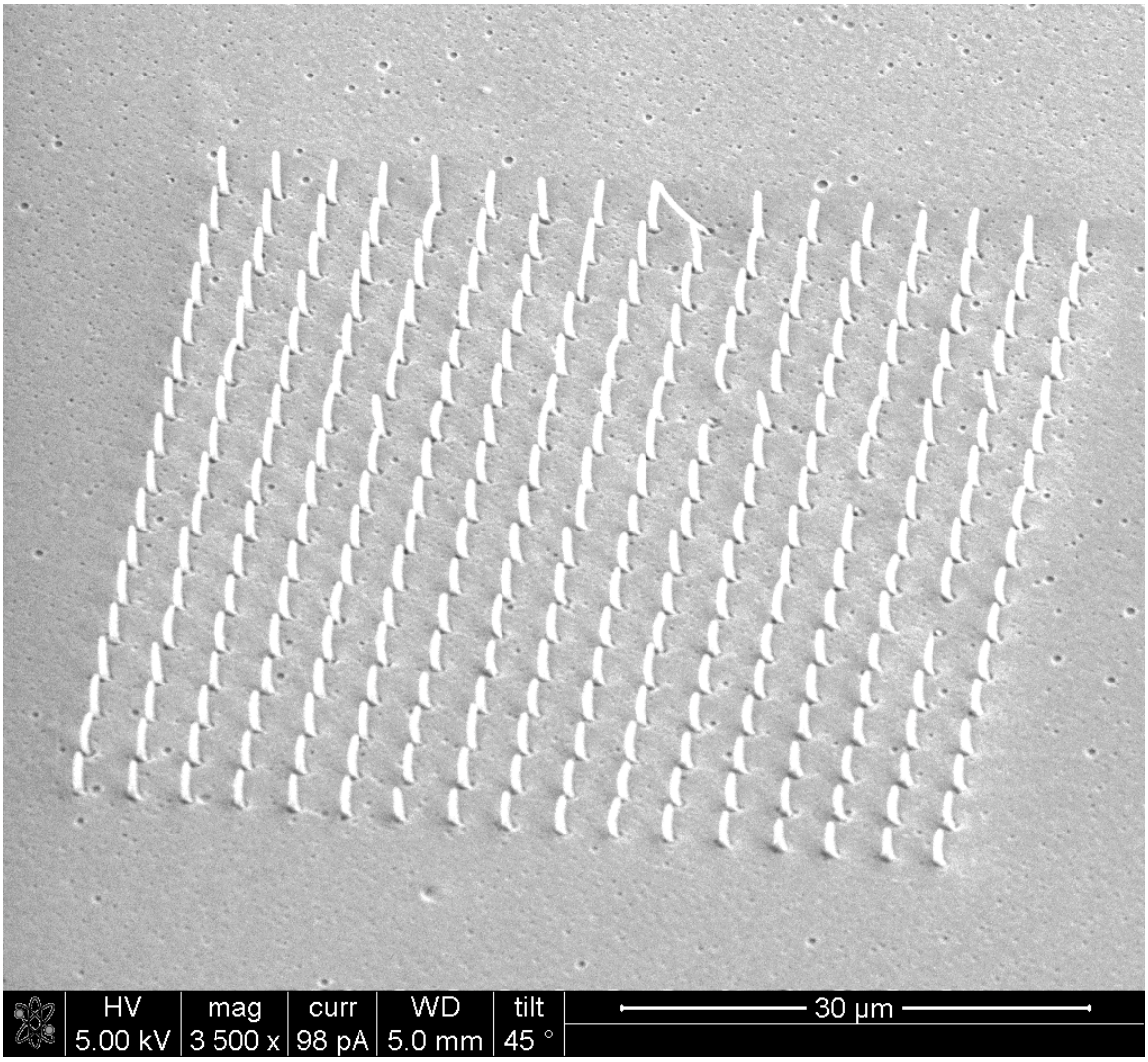

Figure 6.15 An imprint of an array of wells fabricated using single femtosecond pulses focused at the back side. The measured variation in volume is ± 3%.

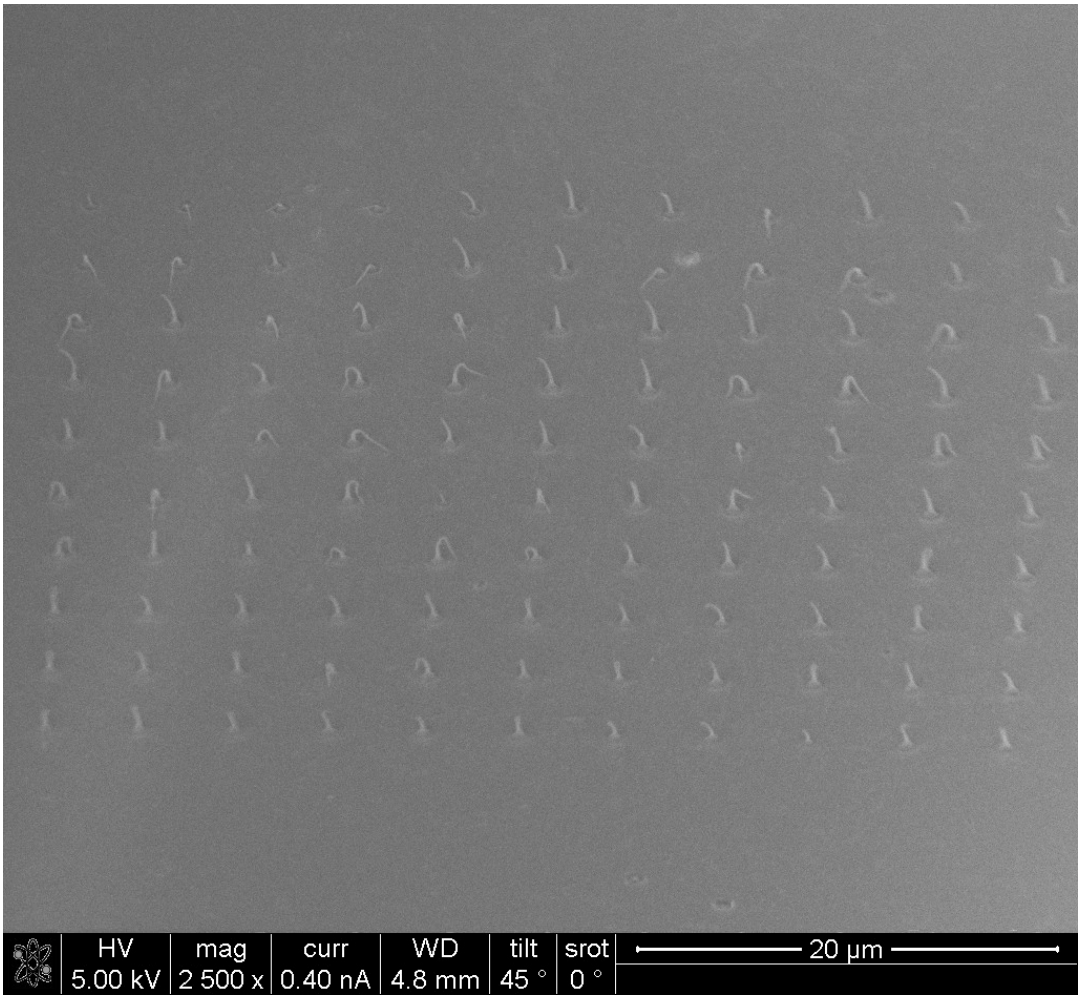

Figure 6.16 An array of front side machined channels for use as wells. These wells exhibit lower volume than the back side nanochannels.

References

Couairon, A. and Mysyrowicz, A. (2007), 'Femtosecond filamentation in transparent media', *Physics Reports-Review Section of Physics Letters,* 441 (2-4), 47-189.

Couairon, A., et al. (2005), 'Filamentation and damage in fused silica induced by tightly focused femtosecond laser pulses', *Physical Review B,* 71 (12), 11.

Herbstman, J. F., Hunt, A. J., and Yalisove, S. M. (2008), 'Morphologies and nonlinear scaling of laser damage on glass surfaces by tightly focused femtosecond pulses', *Applied Physics Letters,* 93 (1).

Joglekar, A. P., et al. (2004), 'Optics at critical intensity: Applications to nanomorphing', *Proceedings of the National Academy of Sciences of the United States of America,* 101 (16), 5856-61.

--- (2003), 'A study of the deterministic character of optical damage by femtosecond laser pulses and applications to nanomachining', *Applied Physics B-Lasers and Optics,* 77 (1), 25-30.

Ke, K., Hasselbrink, E. F., and Hunt, A. J. (2005), 'Rapidly prototyped three-dimensional nanofluidic channel networks in glass substrates', *Analytical Chemistry,* 77 (16), 5083-88.

Keller, U. (2003), 'Recent developments in compact ultrafast lasers', *Nature,* 424 (6950), 831-38.

Kudryashov, S. I., et al. (2007), 'Nanochannels fabricated by high-intensity femtosecond laser pulses on dielectric surfaces', *Applied Physics Letters,* 91.

Liu, W., et al. (2002), 'Intensity clamping of a femtosecond laser pulse in condensed matter', *Optics Communications,* 202 (1-3), 189-97.

McDonald, J. P., et al. (2006a), 'Femtosecond pulsed laser direct write production of nano- and microfluidic channels', *Applied Physics Letters,* 88 (18), 3.

--- (2006b), 'Femtosecond-laser-induced delamination and blister formation in thermal oxide films on silicon (100)', *Applied Physics Letters,* 88 (15), Art.

Schaffer, C. B., Jamison, A. O., and Mazur, E. (2004), 'Morphology of femtosecond laser-induced structural changes in bulk transparent materials', *Applied Physics Letters,* 84 (9), 1441-43.

Shen, Y. R. (1984), *The principles of nonlinear optics* (New York: J. Wiley) xii, 563 p.

White, Y. V., et al. (2008), 'Single-pulse ultrafast-laser machining of high aspect nano-holes at the surface of SiO2', *Optics Express,* 16 (19), 14411-20.

Chapter 7

Conclusions

The application of near threshold, tightly focused, femtosecond laser pulses is a versatile tool capable of manipulating matter on scales down to tens of nanometers. This damage is currently a subject under much study; consequently, there are a number of phenomena generated by tightly focused femtosecond laser damage that are new and interesting.

This thesis examines a few of the novel morphological phenomena that can occur when a tightly focused femtosecond pulse interacts with a glass target. First, it shows that subsurface focusing, under the correct conditions, can lead to blistering effects, even in homogenous, transparent dielectric materials. The shockwave formed during the formation of this femtosecond laser damage can generate enough pressure to remove solid rings or "grommets" of material from the region around the central hole.

Another novel phenomenon that can occur during the interaction of femtosecond lasers and the glass target is the generation of nanochannels, voids several microns long and less than 500 nm wide created from single pulse damage. These channels are highly reproducible and can occur for laser pulses focused at the front side or the back side of the coverslip target. They have been shown to scale with both the pulse fluence and the position of the focus within the target, indicating that the likely mechanism for the generation of these nanochannels is through self-focusing. Nonlinear interaction between the beginning of the pulse and the material serves to refocus the pulse and maintain highly efficient ablation along the axial dimension.

Although seemingly at odds, the synthesis of these two phenomena is a matter of examining the conditions under which the glass is damaged. Grommet formation occurs

for a range of fluences near threshold when the laser focus is a few hundred nanometers below the surface. Nanochannel formation was studied at higher fluences and under conditions where the laser was typically focused more than 500 nm from the surface. As illustrated in Figure 7.1, grommet formation can be observed in acetate replica images for irradiated regions where the focus is near the surface.

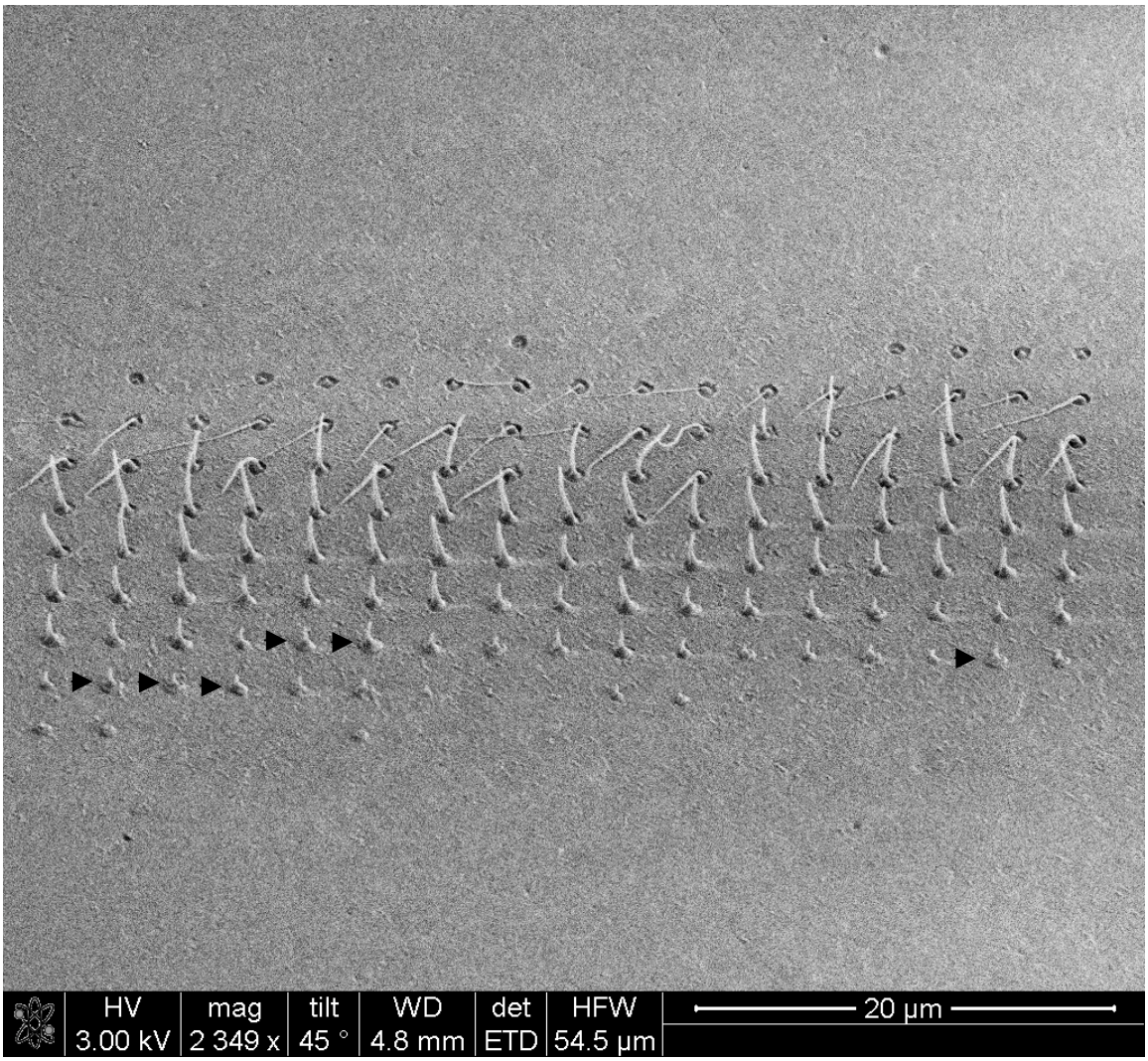

Figure 7.1 Nanochannel formation during back side machining at 67 J/cm^2. Arrows indicate a few of the damage spots where grommet formation is evident.

Future directions for this research involve probing the dynamics of the machining process both experimentally and theoretically. It would be illuminating to perform side imaging pump-probe experiments on grommet formation to examine the dynamics of the grommet

removal process. The speed with which the grommet is ejected from the surface can relate values for the pressures involved with the laser damage process in glass. Pump-probe experiments may also be able to document the self-focusing and filamentation process during the formation of nanochannels, providing direct evidence for this mechanism.

Simulations of this work would also add information about processes on smaller length and time scales that cannot be probed easily with experimental techniques. The tightly focused laser damage system is a difficult one to simulate in that proper simulation must include a large number of physical processes. An accurate simulation should take into account: wave optics, nonlinear optical phenomena, nonlinear ionization and excitation, carrier transport, heat transport, phase changes, shockwave generation and hydrodynamic material effects among many others. For the tightly focused laser system, this must performed in at least 2 dimensions on both high resolution, short time scales during the pulse, as well as longer time scales, as thermal effects take over, to properly replicate the interplay between various effects. One tool that may have the required characteristics would be the HYADES code, simulation software developed for plasma dynamics study.

Although further probing of these phenomena via experimental and theoretical techniques would answer many questions that remain about the dynamics of the laser damage process, the engineering of new applications that take advantage of these damage phenomena has already begun. Applications for the single pulse fabrication of nanochannels are varied and are currently being developed. Some preliminary applications include the generation of large arrays of small volume nanowells for specialized confocal microscopy study and out-of-plane vias for microfluidic technology. Future work studying the use of these nanochannels as nanopores, through-holes for membranes filters, and in other technologies is being developed.

The aforementioned nanochannels are fabricated with single pulses, allowing the machining rate to approach the repetition rate of the laser. Recent developments in laser technology allow for repetition rates over 1 MHz at pulse energies usable for machining

(Keller 2003). This technology allows ultrafast laser machining to compete with photolithographic techniques for patterning structures on small scales. An ideal approach would likely blend the two techniques, allowing the advantages of the two approaches to complement each other.

Furthermore, an exciting new technology has become accessible through this work: nanoimprinting. The acetate replicas that illustrate single pulse nanochannels also represent the ability of laser machining to form a mold such that imprinted fabrication can be performed quickly and easily at the nanoscale. The versatility of laser machining technology allows rapid, precise, and easily configurable structures to be fabricated with features well below one micron. The imprint of these structures can then be used for a range of applications. A simple array similar to that shown in Figure 6.15 could be coated either with metal to form a microreflector or grating. This array could also be coated with antibodies or receptors to create a sensor with a large surface area. These are simple applications utilizing a free standing array of pillars; more complicated surface structures can easily be fabricated using this technology, extending the range of potential applications for imprinting to many other technologies.

Future technologies and applications for ultrafast laser machining at small scales require illumination of physical features and mechanisms that occur during this process. This work presents the results of the study of a number of new phenomena occurring during femtosecond laser damage. Uncovering and explaining novel damage phenomena such as those presented in this thesis allow the boundaries of microscale technology to be expanded to reach ever more new and interesting problems.

References

Keller, U. (2003). "Recent developments in compact ultrafast lasers." Nature **424**(6950): 831-838.